Titre: Title:	A Continuum-Based Fully-Lagrangian Model for Ice-Water Dynamics
Auteur: Author:	Mahyar Talebi
Date:	2022
Type:	Mémoire ou thèse / Dissertation or Thesis
Référence: Citation:	Talebi, M. (2022). A Continuum-Based Fully-Lagrangian Model for Ice-Water Dynamics [Mémoire de maîtrise, Polytechnique Montréal]. PolyPublie. https://publications.polymtl.ca/10483/

POLYTECHNIQUE MONTRÉAL

affiliée à l'Université de Montréal

A continuum-based fully-Lagrangian model for ice-water dynamics

MAHYAR TALEBI

Département des génies civil, géologique et des mines (CGM)

Mémoire

présenté en vue de l'obtention du diplôme de *Maîtrise ès sciences appliquées*

Génie Civil

Août 2022

POLYTECHNIQUE MONTRÉAL

affiliée à l'Université de Montréal

Ce mémoire intitulé:

A continuum-based fully-Lagrangian model for ice-water dynamics

présenté par **Mahyar TALEBI**

en vue de l'obtention du diplôme de *Maîtrise ès sciences appliquées*

a été dûment accepté par le jury d'examen constitué de :

Musandji FUAMBA, président

Ahmad SHAKIBAEINIA, membre et directeur de recherche

David VIDAL, membre

DEDICATION

I would like to dedicate the present thesis to my parents, my wife and my brother for all of their usual support, love, encourage and devotion and above all, to my upcoming girl who has brightened our lives.

RÉSUMÉ

La reconnaissance du comportement dynamique des glaces fluviales est d'une grande importance, en particulier dans les régions froides, où elles ont le potentiel de déclencher les phénomènes dits de blocage des glaces. Étant donné que ces phénomènes sont hautement dynamiques, leur dynamique ne peut être capturée que par des méthodes numériques appropriées. Les méthodes numériques qui traitent les problèmes de la dynamique de glaces sont soit basées sur une représentation discrète ou continue de blocs de glace. Alors que les approches discrètes, telles que la méthode des éléments discrets (DEM) sont très précis, elles demeurent néanmoins coûteuses en ressources informatiques pour des applications à grande échelle car elles traitent de banquises prises individuellement. D'autre part, la description continue offre une scalabilité et est moins couteuse car elle considère un amas de glace comme un seul corps continu et permet de résoudre sur cet ensemble les équations de conservation. En combinaison avec les méthodes numériques lagrangiennes (particules) lissées et sans maillage, telles que le Smoothed Particle Hydrodynamic (SPH) et le Moving Particle Semi implicite (MPS), la description continue peut également offrir un niveau de précision et de flexibilité comparable à la description discrète.

Dans cette étude, nous proposons une méthode numérique lagrangienne MPS pour la simulation de la dynamique multiphasique glace-eau basée sur la description continue de la glace et de l'eau, considérés comme des fluides non-Newtoniens et Newtoniens respectivement. Pour traiter les interactions hautement dynamiques du couple glace-eau, les équations complètes de Navier-Stokes, sans l'hypothèse d'écoulement peu profond couramment utilisée, sont résolues. Pour prédire le comportement non-Newtonien de glace comme milieu continu, nous examinons deux lois de comportement viscoplastiques, à savoir la loi viscoplastique standard (SVP) et la loi de Herschel – Bulkley (HB). Le modèle développé est validé et évalué pour le cas du test de perforation et de l'initiation de l'embâcle. La comparaison avec les données expérimentales montre la précision et la fiabilité du modèle développé.

De manière générale, la contribution de cette étude peut être classée en trois parties :

1- L'application de la méthode MPS est montrée en simulant deux essais expérimentaux et en validant les résultats.

2- L'approche basée sur le continuum s'avère suffisamment précise malgré leurs hypothèses de simplicité.

3- Les modèles rhéologiques visco-plastiques se sont avérés très compatibles avec les méthodes particulaires basées sur l’approche continue.

ABSTRACT

Recognition of the behavior of the river ice dynamics is of great importance, especially in cold regions, as they have the potential to trigger the so-called ice jamming phenomena. Since these phenomena are highly dynamic, its dynamics can only be captured by proper numerical methods. Numerical methods for ice dynamic problems are either based on the discrete or continuum descriptions of the ice floes. While the discrete-based approaches, such as the Discrete Element Method (DEM), are very accurate, they are computationally expensive for large-scale problems, as they deal with individual ice floes. On the other hand, the continuum description offers scalability and computational affordability, by considering the assembly of ice parcels as a body of continuum and solving the conservation equations. In combination with the mesh-free Lagrangian (particle) numerical methods, such as Smoothed Particle Hydrodynamic (SPH) and Moving Particle Semi implicit (MPS), the continuum description can also offer accuracy and flexibility comparable to the discrete description.

In this study, we propose an MPS Lagrangian numerical method for simulation of multiphase, multiphasic ice-water dynamics, based on continuum description of both ice and water, considered as non-Newtonian and Newtonian fluids, respectively. To deal with the highly dynamic ice water interactions, the full Navier-Stokes equations, without the commonly used shallow flow assumption, are solved. To predict the non-Newtonian behavior of the ice continuum, we examine two visco-plastic constitutive laws, i.e., the Standard Visco-Plastic (SVP) and the Herschel–Bulkley (HB). The developed model is validated and evaluated for the case of punch-through test, and ice jam initiation. Comparison with the experimental data shows the accuracy and reliability of the developed model.

In general, the contribution of this study can be categorized into three parts:

1- Application of the MPS method is shown by simulating two experimental tests and validating the results.

2- The continuum-based approach is shown to be accurate enough in spite of their simplicity assumptions.

3- The Visco-Plastic rheological models are shown to have great compatibility with continuum-based particle methods.

TABLE OF CONTENTS

LIST OF TABLES

LIST OF FIGURES

LIST OF APPENDICES

Chapter 1 INTRODUCTION

Recognition of natural phenomena that occur in the system of creation has long attracted much attention. For this reason, many efforts have been made by scientists and researchers in the world to understand the laws governing these phenomena to control and use them in an optimal way for the development of human life. As one of the branches of science, fluid mechanics is no exception, what is considered in this field is modeling, and solving problems related to the flow and behavior of fluids. The complexity and unpredictability of fluid behavior in many engineering phenomena have made it impossible to analyze these occurrences except by increasing the knowledge and deep understanding of universal rules and sciences. One of the challenging issues in this context is having comprehensive knowledge regarding the river ice dynamics. It is most important in cold regions since in some cases, it can have harmful effects. The ice jamming phenomenon is one of those issues which every year, all of the cold regions like Canada are dealing with. Since in these regions the rivers are frozen in winter times, by increasing the temperature in spring, it starts melting and forming pieces of ice called ice floes which can run along the river bed. These ice chunks can stuck in their way when there are obstacles like bridges or when the river bed gets narrow. In this case, they can be accumulated for kilometers and act like a dam which increases the water level and causes a flood. One of the recent ice jam floods is on April 2020 which developed on the Athabasca River in Canada leading to the flooding of Fort McMurray. European Union's Copernicus provided satellite data which lends a hand to monitoring river ice conditions. Figure 1.1 shows the extent of flooding. This ice jam displaced 13000 people and damaged 1200 properties. Another example of this phenomenon is on January 2018 along the Connecticut River in Haddam (USA) which causes kilometers of ice jam along the river. Figure 1.2 which is also provided by European Union's Copernicus shows the extent of it. Only a few examples of recent ice jams in Canada include the Town of Peace River along the Peace River in Alberta (Lindenschmidt, Das, Rokaya, Chun, & Chu, 2015), Winnipeg, and Selkirk on the Red River in Manitoba (Lindenschmidt, Sydor, Carson, & Harrison, 2012) and Raymond on the St. Anne River in Quebec (Turcotte & Morse, 2015).

Figure 1.1 Ice jam flooding in Fort McMurray (Ref: European Union's Copernicus)

Figure 1.2 Ice jam flooding in Connecticut River (Ref: European Union's Copernicus)

In general, there are two different perspectives predicting the behavior of fluids in empirical ways, which are usually time-consuming and costly, and theoretical methods. The theoretical methods can in turn be divided into numerical and analytical methods. Each of these perspectives has its advantages and disadvantages, and in general, both are complementary. With the advancement of physics and mathematics, the theoretical method for the theoretical study of phenomena related to fluids has received more attention. In examining the theory, it is first necessary to identify the significant factors and their importance and provide a physical model for the phenomena. Based on this model, the governing mathematical relations are identified, and the problem is formulated. Due to the complex nature of fluid dynamics, the analytical methods can only be useful for simplified physics which is in most cases far from the real phenomena and many factors are neglected. On the other hand, the numerical methods are being improved significantly and are containing more and more aspects of the real phenomena to have much more precise simulations, especially with the advancement of computers. Numerical or analytical methods or a combination of both can be used to solve the governing equations.

As mentioned earlier, complex problems cannot be handled by analytical solutions. As ice dynamics-related problems have a very complex nature, they need to be dealt with advanced numerical solutions. Particle-based methods are relatively modern approaches that are most suitable for highly dynamic problems. In the following sections, you may find detailed descriptions of these methods and their advantages over conventional methods in coping with such unpredictable phenomena.

1.1 Numerical simulation

The main idea of creating numerical simulations is related to the necessity of interpreting physical problems by numerical models. While performing the experiments is mostly expensive and time demanding, with the advancement of computers, Numerical simulations have quickly become critical methods for solving complex engineering problems. Figure 1.3 show the relationship between numerical, experimental, and theoretical solutions and the process of numerical simulation (G.-R. Liu & Liu, 2003).

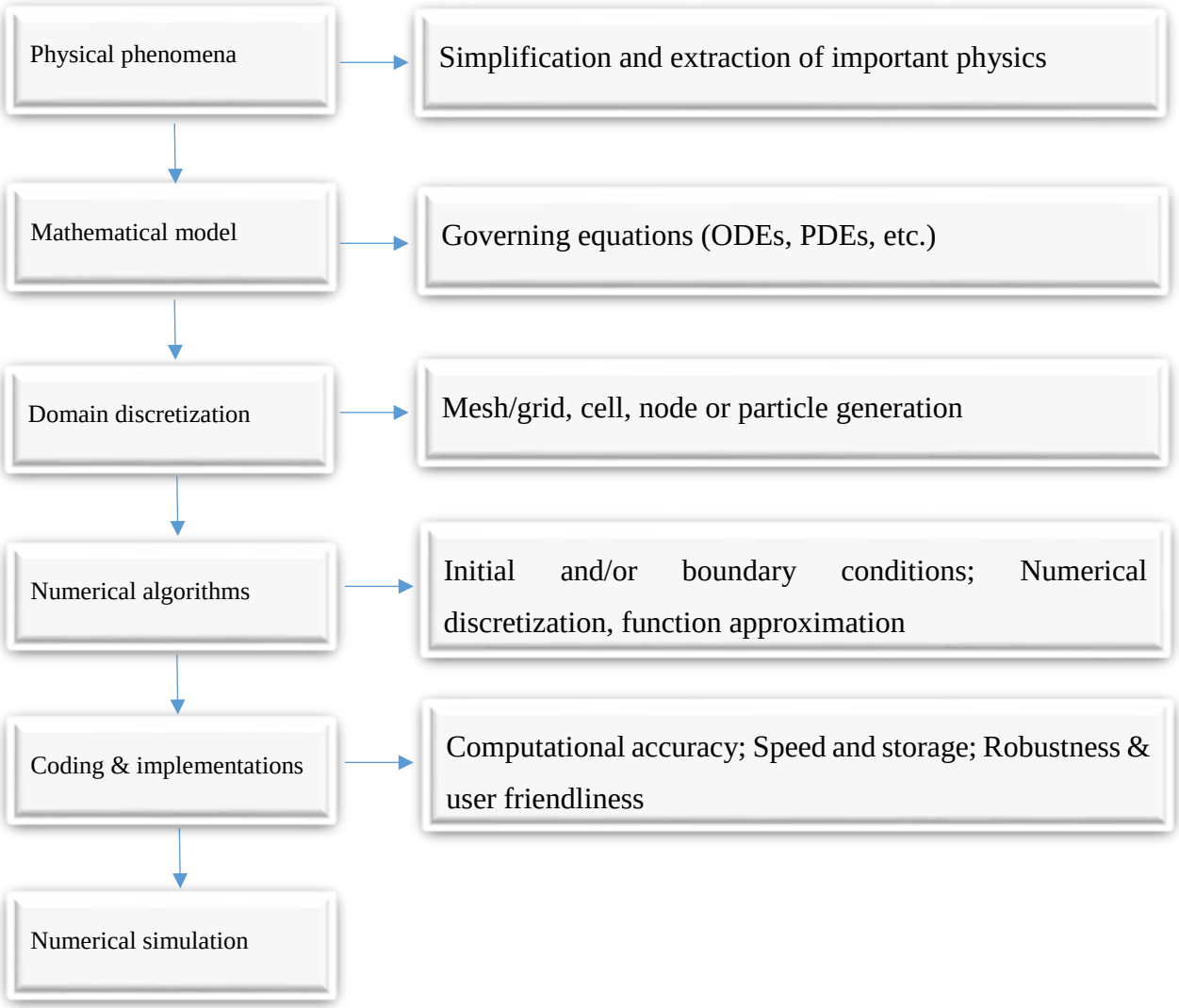

Figure 1.3 Procedure of conducting a numerical simulation [1]

As is shown in Figure 1.3, a numerical simulation contains an appropriate understanding of the problem physics and constraints, knowing the governing equations, discretizing the domain into infinitely small parts, utilizing proper algorithms, coding and implementing the algorithms, and finally having the results of the numerical simulation.

1.2 Main approaches in computational fluid dynamics

Discretization can be nominated as one of the main processes in the numerical methods. By discretizing, the freedom degree of the governing differential equation reduces from infinity to a finite degree. Hence, there is only needed to determine the solution for specified locations and times which can be solved using computers.

Generally, there are two different points of view to describe a physical governing equation: the Lagrangian and the Eulerian methods. The Lagrangian method is a material description that is typically represented by the finite element method (FEM) (Zienkiewicz, Taylor, & Zhu, 2005), while the Eulerian method is a spatial description and is typically represented by the finite difference method (FDM) (Forsythe & Wasow, 1960). Choosing either of these methods for the problems depends mostly on the problem's characteristics (Z. Zhang & Chen, 2007). To discretize the problem domain, we have two main approaches that are described in the following.

1.2.1 Mesh-based methods

The mesh-based or grid-based methods discretize the computational domain using mesh. These meshes can either be static or dynamic, which causes different types of grid-based methods, namely the Eulerian, the Lagrangian, and the Eulerian-Lagrangian (Spandan, Lohse, de Tullio, & Verzicco, 2018) mesh-based methods. The **Eulerian mesh-based** methods, Which are known as conventional methods, are well-developed methods that have been utilized vastly in solid and fluid mechanics (Dunne, 2006). Despite the widespread use and remarkable success of these methods, they face inherent difficulties and limitations in modeling flow with large deformation, such as wave breaks in seas and violent river flows (Shakibaeinia & Jin, 2010). These methods' main feature is dividing a continuous domain into small discrete parts during the meshing process. Meanwhile, the mesh is kept constant in space and does not change by changing the object's location.

Unlike the Eulerian mesh, in the **lagrangian mesh-based methods** like the well-known FEM method, the grid is attached to the material and moves with the object movement (G. R. Liu & Jerry, 2003). It can be noted that the Lagrangian mesh has advantages over the Eulerian one. Since

there is no convective term in the Lagrangian framework, the code will become conceptually simpler, and also by attaching the nodes to the material, tracking the history of field variables becomes easier. (Figure 1.4).

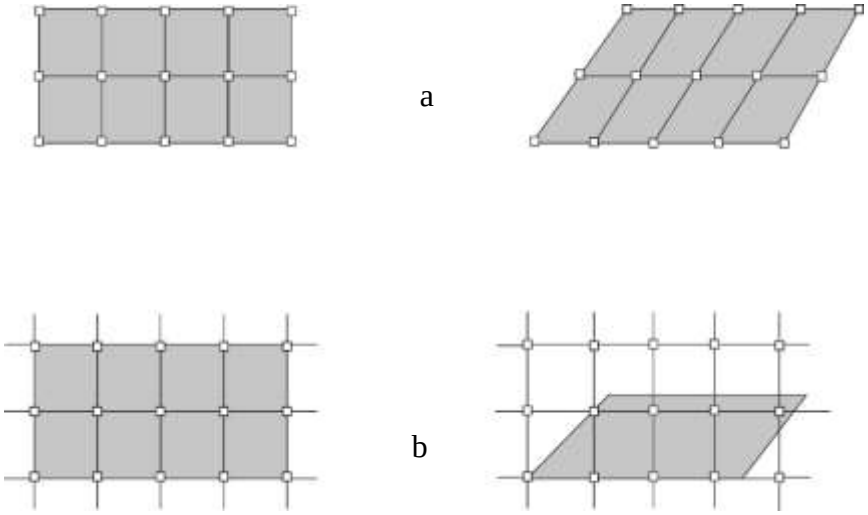

Figure 1.4 (a) Lagrangian mesh (b) Eulerian mesh

Combining the methods above leads to more computationally beneficial methods that use each method's advantages. The Coupled Eulerian-Lagrangian (CEL) (Mair, 1999) and the Arbitrary Lagrange Eulerian (ALE) (Benson, 1992) have resulted from this combination.

1.2.2 Meshless methods

Although there are many developments in Mesh-based methods in academic and industrial applications, a more recent generation of computational methods is attracting interest; Mesh-free or Meshless methods, which have many advantages over conventional Eulerian methods (Gotoh & Khayyer, 2016). For the Mesh-based Methods, due to the grid-based interpolations, low-quality meshes can lead to high errors which need re-meshing which is very common for complex problems. This process is highly time and labor-consuming, not even feasible for some three-dimensional problems (Nguyen, Rabczuk, Bordas, & Duflot, 2008). Nowadays, scientists are

paying attention to developing a generation of meshless methods that are expected to have an advantage over conventional grid-based methods such as finite element and finite difference methods. Meshless methods include some common tools with the former but differ in the meanings of the approximation and the method of application.

The beginnings of Meshless methods may go back to a few decades ago, but the most significant advances in this field were in the 1990s. The Meshless method is a method that, unlike Eulerian methods, does not require grid definition or computational domain discretization. In this method, a number of nodes (particles) that are scattered both in the computational region and on the computational boundary are used. These nodes (particles) do not have a grid shape, i.e., no prior information about the relationship between nodes (particles) is needed to interpolate or approximate the functions of the variables. For a detailed review of mesh-free methods see (G.-R. Liu, 2009)

1.3 Advantages of meshless methods over mesh-based methods

Undoubtedly, the ability of meshless methods in modeling complex flows has attracted increasing attention from researchers to these new methods (Yan, Mohammadian, & Rennie, 2020). Some of the advantages of these new and practical methods can be expressed as follows:

- Flow domain discretization is made by particles which do not have any connectivity to each other.
- Complex geometries can be simulated by initial discretization, i.e. setting up particles in the initial condition.
- Since each particle carries the properties of the fluid, it can be traced to the properties of the fluid at that point. Also, obtaining deformation boundaries and free surfaces will not be a complicated task.
- Correcting and recreating particles is easier than correcting the entire computational domain of the mesh.

Moreover, numerical diffusion is unavoidable in mesh-based methods (Gotoh & Sakai, 2006). Unlike the Eulerian method, each particle is defined on the object, and its location changes as the object moves. When the body is highly deformed and the structure is not naturally shaped, the accuracy of the relationship and its resolution is greatly affected and it is difficult to apply the mesh-based Lagrangian method.

1.4 Typical mesh-free methods

Providing more accurate and stable numerical solutions for the PDE's and facilitating the analysis of complex geometries can be nominated as the main purposes of the relatively modern mesh-free methods. Here are some of the most popular meshless methods which all share some common features but are still different in the implementation process.

One of the most famous methods that are used widely in fluid and solid mechanics is Smoothed Particle Hydrodynamics (SPH) developed by Gingold, Monaghan (Gingold & Monaghan, 1977), and Lucy (Lucy, 1977) in 1977. It was initially played out to deal with astrophysical problems, however, its applications are diverse nowadays in wave-structure interaction, geophysical flows due to landslides, nuclear sludge flows, welding, gearbox flows, and many others (Lind, Rogers, & Stansby, 2020). One may find many recent reviews on this method (Violeau & Rogers, 2016; Z.-B. Wang et al., 2016; Ye, Pan, Huang, & Liu, 2019).

The moving particle semi-implicit (MPS) method is also another mesh-free method. It was first developed by Koshizuka, et al (1995) and originally designed to model fluid flow problems by providing an approximation of flow PDE's based on integral interpolations. Rapidly, This method introduced a set of simple models for the derivatives in the flow equation according to a local weighted averaging algorithm (Xie & Jin, 2016). This method has also been applied to a vast range of both fluid flow (e.g. (Shakibaeinia & Jin, 2011)) and other engineering problems. The MPS method of spatial derivatives is only based on a local weighted averaging process that does not deal with the gradient of the kernel function, which in turn, resolves the instability issues originating from the kernel function derivatives in the original SPH formulation and that would be the basic difference between MPS and SPH (Shakibaeinia & Jin, 2012). Also, Thanks to the non-dimensional

particle number density instead of the real density, the density discontinuity at the phase interfaces of multiphase simulations are resolved (Hu & Adams, 2006). A bunch of recent hydro-environmental been developed using MPS and SPH methods (Amaro, Cheng, & Buruchenko, 2021; Khayyer, Tsuruta, Shimizu, & Gotoh, 2019; Snelling, Collins, Piggott, & Neethling, 2020)

Unlike the SPH and their corrected adaptions that were strong form based, many other methods developed in the 1990s in a weak form which were mostly dealing with solid mechanics (Garg & Pant, 2018). The extended finite element method (XFEM) eliminates the need for re-meshing in the FE method (Belytschko & Black, 1999) and has many applications in the analysis of variations of fracture problems (Pathak, Burela, Singh, & VirSingh, 2015; Shedbale, Singh, & Mishra, 2013), Reproducing kernel particle method (RKPM) which is developed to remove the instabilities in SPH method (W. K. Liu, Jun, & Zhang, 1995) and Mesh-less local Petrov-Galerkin (MLPG) that has excel to other techniques since no Shadow elements and no special procedure for integration is needed (Atluri & Zhu, 1998) are only a few developed particle-based methods. Numerical manifold method (NMM) (Tsay, Chiou, & Chuang, 1999), cracking particle method (CPM) (Rabczuk & Belytschko, 2004) and Iso-geometric analysis (IGA) (Nguyen, Anitescu, Bordas, & Rabczuk, 2015) can be nominated as other practical meshless methods.

1.5 Past ice dynamic experiments

Table 1.1 shows the experiments that have been done so far in the context of river ice dynamics. Since the experimental situation and dealing with ice is tricky and hard, the experiments done in this context are a bit scarce.

Table 1.1 Past experiments in the context of river ice

	Channel geometry				Ice floes properties			
Reference	**Length (m)**	**Width (m)**	**Height (m)**	**Ice control structure**	**ice Material**	**floe shape**	**Density $\left(\frac{Kg}{m^3}\right)$**	**Equivalent diameter (cm)**
(Hopkins & Tuthill, 2002)	36	2.25	0.18	Ice boom	Real ice	Angular	920	13.5
(Healy & Hicks, 2006)	32	1.22	0.91	Mesh	Polyethylene	Cube	952-965	3.1
(Lucie, Nowroozpour, & Ettema, 2017)	14.63*0.254*0.203 + (25.9*0.254*0.203) Sinuous channel			No	Polyethylene & Polypropylene	Bead & Block	905-952	1.77
(Morse, Francoeur, Delcourt, & Leclerc, 2006)	15	1.5	0.22	Pier/Net and boom/net	Polyethylene	disks	917	1.27-5.7
(J. Wang et al., 2019)	26.68	0.4	0.2	No	Polyprsopylene	Cube	918	2-6

1.6 Existing models

In order to simulate a highly dynamic and large-scale phenomenon such as an ice jam, an appropriate model is needed. Some existing models in this context are as follows:

Table 1.2 Existing models in ice dynamics simulation

Models		Discrete/ Continuum?	Framework	Example model/reference	Pros/cons.
Water hydrodynamics	Ice dynamics				
1D depth-averaged FVM/FDM	Advection-diffusion	Continuum	Eulerian	RIVICE (Lindenschmidt, 2017)	✓ Practical for large scales × Simplified and not detailed
2D depth-average FVM	2D depth-averaged SPH or MPS	Continuum-Continuum	Eulerian-Lagrangian	SPH-FVM DynaRICE (Shen, Su, & Liu, 2000) MPS-FVM (our ongoing work)	✓ Practical for large scales × Depth-averaged →not good for highly dynamic conditions
1D,2D, 3D Eulerian or Lagrangian	2D/3D DEM	Continuum-Discrete	Eulerian-Lagrangian Or Fully-Lagrngian	CFD-DEM (Hopkins, 2002) MPS-DEM (Junior, Mellado-Cusicahua, Shakibaeinia, & Cheng, 2021) SPH-DEM (Billy et al, 2022)	✓ Detailed ice dynamic × Expensive
2D/3D SPH or MPS	2D/3D SPH or MPS	Continuum-Continuum	Fully Lagrangian	Fully Lagrangian MPS **(current study)**	✓ Detailed (full-dynamic) ✓ A bit expensive, still practical

As provided in Table 1.2, several models can handle the ice dynamics with their advantages and limitations. The first model uses the advection-diffusion for the ice dynamics in one dimension and a depth-averaged FVM or FDM for the water phase. Although it is computationally affordable and can mimic some river ice processes such as ice generation, ice transport, and ice cover progression,

these models are not able to capture some ice details such as viscosity (Lindenschmidt, 2017). Some other models simulate the ice phase with a two-dimensional depth-averaged SPH or MPS method and utilize the FVM method for the water phase. These models are Eulerian-Lagrangian ones with a continuum approach, which are a bit more expensive than the first group yet still affordable but they suffer from a lack of details and are not suitable for highly dynamic cases (Shen et al., 2000). The third group simulates the ice phase with the DEM method which is capable of handling the details of each ice floe individually and provides very accurate results. This method can be coupled with any Lagrangian or Eulerian model to simulate the ice-water dynamics. The issue with these models is their affordability. Since we are dealing with large scales, using the DEM method can not be considered as a good choice. The last group models both water and ice phases using Lagrangian particle-based methods like MPS or SPH with a continuum approach.

Considering the pros and cons of each model, one can find that a continuum-based fully Lagrangian model would be the best fit for our purpose since it takes care of affordability and precision at the same time.

1.7 Continuum-based approach

The main concept behind the continuum theory is mostly appropriate for the large-scale sea ice evolutions but studies have shown that the continuum assumption is still useful. In this study, we assume the ice parcels and the water between the ice parcels as a body of continuum. This assumption offers scalability and computationally affordability while taking care of reasonable accuracy.

A recent study by Hutter and Losch (Hutter & Losch, 2020) showed a great agreement between their model results and observations for many drift and deformation feature statistics at relatively low resolutions. Many other studies have also shown that continuum Visco-Plastic and Elastic Visco-Plastic models can accurately simulate key sea ice properties like large-scale distributions of sea ice thickness, concentration, and circulation (Kreyscher, Harder, Lemke, & Flato, 2000); relationships between sea ice concentration, thickness, and velocity (Docquier et al., 2017); and long-term trends in winter sea ice velocity (Blockley et al., 2020; Tandon, Kushner, Docquier,

Wettstein, & Li, 2018). A continuum-based approach to ice-water interactions using a Lagrangian method is the idea behind this research.

All of the simulations of this study are based on the continuum assumption of the ice particles.

1.8 Numerical particle-based modeling of ice dynamics

One of the natural phenomena's that happens in cold regions and recently attracted researchers' interests is the ice jamming phenomenon. As ice can be considered a non-Newtonian fluid, having a detailed study of this destructive issue is of high interest to this research.

Ice-modeling problems can be solved analytically for a certain and limited number of cases like sea-ice growth (Leppäranta, 1993), but generally flow pattern, ice temperature, thickness, and rheology are limitations that ice-sheet models need to deal with and augment the necessity of ice numerical modeling (Rybak & Huybrechts, 2003). In computational fluid dynamics, many mesh-based numerical methods have been developed to solve and study different fluid flows. Usually, the main purpose of using these methods is to solve the Navier-Stokes equations. Although these methods have shown their effectiveness in simulating many problems, they have encountered difficulties in dealing with relatively complex ones that have free surfaces, boundary deformation, large deformation, and so on. Generating an appropriate mesh in mesh-based methods for complex geometries is not a simple task and usually involves complicated and time-consuming processes. In addition, with mesh-based methods, finding accurate free surfaces and moving boundaries is challenging (A. J. C. Crespo, 2008). Thus, a relatively newer approach known as Lagrangian particle-based methods is taking care of these complex problems. Moving particle semi-implicit (MPS) is among the well-developed Lagrangian methods employed in continuum-based modeling of Newtonian and non-Newtonian fluids (Shakibaeinia & Jin, 2011) and is widely used in numerous hydrodynamic problems (Duan, Yamaji, & Koshizuka, 2019; Nodoushan, Shakibaeinia, & Hosseini, 2018). The weakly compressible MPS introduced by Shakibaeinia and Jin (Shakibaeinia & Jin, 2010) which employs an equation of states instead of solving Poisson's Pressure Equation (PPE) is implemented in the current study.

The instability and accuracy issues especially in pressure fields are known to be associated with these particle-based methods and many efforts have been done to tackle these issues (Khayyer, Gotoh, & Shimizu, 2019; C. Zhang, Xiang, Wang, Hu, & Adams, 2019). Many enhancement algorithms like artificial diffusive terms (J. J. Monaghan, 1994), higher order approximations (Tsuruta, Khayyer, & Gotoh, 2013), and particle stabilizing and regularization techniques (Lind, Xu, Stansby, & Rogers, 2012) are also introduced and implemented to improve the stability of particle methods. Jandaghian and Shakibaeinia (M Jandaghian & Shakibaeinia, 2020) had a detailed study on the recent improvements in the accuracy and stability of particle methods namely MPS and SPH.

Winter ice cover is an issue, which almost all of the Canadian waterways deal with. A natural phenomenon of these ice cover's melt can be seen each year in the spring, which leads to their break up into ice parcels. The resulting ice floes can sometimes have harmful impacts on the sediments of the riverbeds by eroding them and damaging the structures along their way which also leads to a complete change in the hydrodynamic regime of the river. The flow resistance increase results in the water's depth increase, which itself leads to severe flooding. Accumulation of the ice floes can result in kilometers-long ice jams and significant rises in water levels. The breakup of the ice jams and sudden release of these ice floes can create a flood wave comparable to that of a dam break which in turn can threaten the infrastructures like bridges, buildings, and roads (Beltaos, 2010). Considering its significant impacts, prediction, and understanding of river ice dynamics are very important.

River ice is made up of moving, growing, or melting irregular pieces of ice that can range in size from a few meters to tens of kilometers in length (Hopkins, Frankenstein, & Thorndike, 2004). The importance of glacier and ice sheet dynamics is debatable since they have several significant impacts that cannot be neglected. Because of the considerable reduction in sea ice volume and increased maritime activity in the Arctic Ocean over the last few decades, a reliable sea ice forecast has become a critical component of the region's data assimilation systems (Panteleev, Yaremchuk, Stroh, Francis, & Allard, 2020). Their interaction with the global climate and their contribution to sea-level rise (Chiang & Bitz, 2005; Church et al., 2013), ice runs, and ice jams that can damage hydraulic structures and cause excessive shoreline erosions and also lead to severe flooding by reducing flow cross-section (Shen et al., 2000), and shaping landscapes (Ahlkrona & Shcherbakov,

2017) are only a few of their essential roles in our environment. Beltaos developed the ice jam theory based on the static equilibrium of floating accumulations of granular ice (Beltaos, 1995) and Flato and Gerard computed a static ice jam profile using a one-dimensional numerical model (Flato & Gerard, 1986). In these static ice jam models, the momentum effects of ice and water flows as well as the dynamics of the motions were not considered so they were not able to deal with any information on formation of the ice jams.

The important aspect of ice modeling is the relationship between the sea ice stress, which can be caused by ice floe interactions, to the large-scale deformation of the ice cover, the state of ice cover, and the material properties of sea ice that are all known as the ice rheology (Feltham, 2008).

Early studies show that sea and glacial ice can be considered as a granular material with bulk rheology which is determined by the geometry of ice floes as well as the local mechanics (Feltham, 2005; Hopkins & Thorndike, 2006) and can be described as a non-Newtonian, incompressible and very viscous fluid (Ahlkrona & Shcherbakov, 2017). The very first models of ice rheology, like what Ruzin (Ruzin, 1959) and Reed&Campbell (REED & CAMPBELL, 1960) proposed, were based on parameterizing the stress using a Laplacian operator which effectively treats the ice cover as a viscous fluid. By observing the flow with weak horizontal divergence, Rothrock (Rothrock, 1970) included a pressure term to prevent unrealistic convergence. Further investigations on ice rheology lead to considering the ice as an elastic-plastic (Coon, Maykut, & Pritchard, 1974) and viscous-plastic (Hibler III, 1979) material, and several well-known models like Standard Visco-Plastic (SVP), Granular material approach (GRAM) (Tremblay, 1999).

1.8.1 Sea Ice rheology

In the previous section, the importance of rheology was discussed. Ice rheology is a crucial component of the momentum balance that regulates the dynamic characteristics of sea ice. It defines the link between ice internal stress, deformation, and mechanical strength. Most of the sea ice dynamic models that are currently being used are based on a viscous-plastic (VP) rheology (J.-F. Lemieux et al., 2010) followed by its Elastic numerical approximation formulation (Hunke & Dukowicz, 1997). One reason for the popularity of these models is that sea ice behaves as a plastic material on large scales. Also, their numerical implementation ease of use, and relatively acceptable

results in simulating the ice thickness and motion can be nominated as another fact for their wide usage. These rheology models provide physically acceptable and numerically feasible solutions for modeling sea ice dynamics. Some examples of VP rheology based models are the researches conducted by Heimbach et al (Heimbach, Menemenlis, Losch, Campin, & Hill, 2010), Vancoppenolle et al (Vancoppenolle et al., 2009) and Massonnet et al (Massonnet, Fichefet, & Goosse, 2015). The main rheological model used in this study is the Visco-plastic model proposed by Hibler (Hibler III, 1979). This model is patterned after the Arctic ice dynamics joint experiment (AIDJEX) developed by Coon et al. (Coon et al., 1974) and is not as detailed as AIDJEX but due to its relatively simplicity is more practical which in turn allows to have larger time steps and makes it easier to handle the boundaries. In addition, in terms of comparison, the Herschel–Bulkley (HB) model, which is mostly used for the granular flows in the literature, is also investigated.

Despite the efforts on the continuum-based approach of numerical models for simulation of river ice using Eulerian mesh-based methods (Bai, Zhang, & McGovern, 2017; Sayeed, Colbourne, & Molyneux, 2018), some recent efforts regarding the ice dynamics modeling using particle-based methods have been made. For instance, Nolin et al. simulated ice jamming formation and release using the SPH ice rubble model (Nolin, Roubtsova, Morse, & Quach, 2009), Junior et al. simulated the ice-wave dynamics in which all the motions of an ice floe are captured using the coupled DEM-MPS method (Junior et al., 2021), Liu et al simulated the ice-water interaction by coupling the bond-based peridynamics model for ice and the updated lagrangian particle hydrodynamics (ULPH) for the water phase (R. Liu, Yan, & Li, 2020), Woo et al put their efforts on ice fracture modeling using the maximum normal stress theory for the criterion of fracture by utilizing MPS method (Ren, Sin, Kim, Park, & Jeong, 2020) but in general, due to the complexity of the river ice dynamics, the data obtained are limited, scarce and insufficient. Using the MPS method with a continuum-based approach by taking advantage of rheological models to simulate non-Newtonian fluids, namely ice, is a study that has not been conducted before and is the focus of this study.

1.9 Research objective

The global objective of this study is to develop a continuum-based mesh-free Lagrangian model, based on the MPS method, for the study of river ice dynamic problems.

The specific objectives of this research are:

a) Developing an MPS numerical model for the continuum-based simulation of ice dynamics problems and its validation and calibration using a benchmark case.

b) Investigating the role of different rheological models, such as the Standard Visco-Plastic (SVP) and the Herschel–Bulkley (HB), on the accuracy of ice dynamics predictions.

c) Application and evaluation of a model for the case of ice jam formation, in comparison with the experimental results.

d) Investigating the role of various numerical and physical parameters on the simulation results

1.10 Thesis structure

The present thesis contains five chapters. The first chapter is an introduction of the goal of this study and a literature review of what has been done so far in this context. The second chapter talks about the fundamentals and formulations of the main method which is utilized in the current thesis, namely the MPS method. The third chapter describes two different rheological models (SVP and HB) that are implemented and applied on two test cases, Punch through and ice jam, and the results are validated. The last chapter is the conclusion of this research in which the key findings, as well as the recommendations, are listed.

Chapter 2 FUNDAMENTALS OF THE MPS METHOD

Navier-stokes equations are the well-known governing equations in fluid mechanics motion which relate pressure, velocity, density and other quantities. It consists of two coupled nonlinear partial differential equations, the conservation of mass and the conservation of momentum with Newton's viscosity. The derivative with respect to time in the Lagrangian framework can be expressed as:

$$\frac{D\rho}{Dt} = \frac{\partial()}{\partial t} + (\mathbf{u}.\nabla)() \tag{2.1}$$

This is also called the material derivative which indicates that the amount of change of a variable in time can be described by a temporal and a spatial change. Hence, the Lagrangian form of the Navier-Stokes equation for an incompressible flow can be derived as follows:

$$\begin{cases} \frac{1}{\rho}\frac{\mathrm{D}\rho}{\mathrm{D}t} + \nabla.\mathbf{u} = 0 \\ \rho\frac{\mathrm{D}\mathbf{u}}{\mathrm{D}t} = \nabla.\mathbb{T} + \mathbf{f} \\ P = f(\rho) \end{cases} \tag{2.2}$$

In the equation (2.2) ρ, $\mathbf{u}$, P, $\mathbb{T}$ and $\mathbf{f}$ are density, velocity vector, pressure, total stress tensor and gravity acceleration respectively. It is notable that the convective acceleration, which is considered a source of error in the Eulerian system, is omitted in the Lagrangian framework. To solve these equations, a method should be used to approximate spatial derivatives.

2.1 Interpolations and Kernel function in MPS

The moving particle semi-implicit method, like many other particle-based methods, is based on a local averaging of quantities and vectors. As stated, each particle in MPS can be thought of as a real particle with volume, mass, and pressure. When Particles come closer to each other from a predetermined distance, affect each other and it is said that there is an interaction between them. This distance is called the smoothing length. For each particle, an impact range is defined, denoted by r_e. Smoothing length is one of the characteristics of each particle. In incompressible flows, the

impact range of the particles is normally constant and equal to each other and also equal to the smoothing length, but in compressible flows, it is better to have a different impact range of particles with the smoothing length equal to the average of their impact range.

The arrangement of particles in the initial state is usually normally distributed and the initial particle distance is denoted by δ. The ratio of the smoothing distance to the initial particle distance r_e/δ is an important parameter. The higher its value, the more particles will be contained in the impact range of a particle.

So far, The effect of two particles on each other is mentioned, but the extent of this effect is not discussed. This value depends on a function called the kernel function, which is actually a weight function, and determines how well two particles affect each other. This function is usually denoted by W. The magnitude of this function depends on two variables, the distance between the two particles and the smoothing length:

$$W = W(\vec{r}, h) \tag{2.3}$$

Unlike the SPH method, the MPS method can adopt non-differentiable kernel functions. Below, you may find some popular kernel functions used in the MPS method:

Table 2.1 Formulation of different kernel functions

3rd order polynominal spiky function by Shakibaeinia & Jin, 2010 (Shakibaeinia & Jin, 2010)	$W(r,h)=\begin{cases}(1-\left(\frac{r}{h}\right)^3 & \frac{r}{h}\le 1\\ 0 & \frac{r}{h}>1\end{cases}$
Rational function by Koshizuka and Oka, 1998 (Koshizuka, Nobe, & Oka, 1998)	$W(r,h)=\begin{cases}\left(\frac{r}{h}\right)-1 & \frac{r}{h}\le 1\\ 0 & \frac{r}{h}>1\end{cases}$
Second order polynomialfunction by Koshizuka and Oka, 1996 (Koshizuka & Oka, 1996)	$W(r,h)=\begin{cases}2-\left(\frac{2r}{h}\right)^2 & \frac{r}{h}<1/2\\ \left(\frac{2r}{h}-2\right)^2 & \frac{1}{2}\le\frac{r}{h}<1\\ 0 & \frac{r}{h}\ge 1\end{cases}$
Belytchko et al, 1996 (Belytschko, Krongauz, Organ, Fleming, & Krysl, 1996)	$W(r,h)=\begin{cases}(1-\left(\frac{r}{h}\right)^3 & \frac{r}{h}\le 1\\ 0 & \frac{r}{h}>1\end{cases}$
Lee et al, 1982	$W(r,h)=\begin{cases}\frac{40}{7\pi h^2}\left(1-6\left(\frac{r}{h}\right)^2+6\left(\frac{r}{h}\right)^3\right) & \frac{r}{h}<\frac{1}{2}\\ \frac{10}{7\pi h^2}\left(2-2\frac{r}{h}\right)^3 & \frac{1}{2}\le\frac{r}{h}<1\\ 0 & \frac{r}{h}\ge 1\end{cases}$

As it is obvious in all of the above kernel functions, their value is zero out of the kernel radius. The stability is an issue, which relates to the type of kernel function, as some of them are highly sensitive.

The definition of particle number density in MPS is as follows:

$$\langle n \rangle_i = \sum_{i \neq j} W_{ij} \tag{2.4}$$

The subscript i and j denote a specific particle and the particles in its support domain respectively. It shows that the particle number density is the summation of the kernel values of the adjacent particles of that specific particle. The MPS approximation of an arbitrary function is expressed as follows:

$$\langle f \rangle_i = \frac{\sum_{i \neq j} f_j W_{ij}}{\sum_{i \neq j} W_{ij}} \tag{2.5}$$

In order to satisfy the continuity equation, the particle number density for an incompressible fluid should remain invariant (Koshizuka et al., 1998). A reference particle number density value which is denoted as n_0 can be used as a normalization factor which would reformulate the Eq. (2.5) as:

$$\langle f \rangle_i = \frac{1}{n_0} \sum_{i \neq j} f_j W_{ij} \tag{2.6}$$

One can also obtain the number of particles in a unit volume using:

$$\langle N \rangle_i = \frac{\langle n \rangle_i}{\int_v W(r,h) dv} \tag{2.7}$$

Then the fluid density can be expressed as:

$$\langle \rho \rangle_i = m \langle N \rangle_i = \frac{m \langle n \rangle_i}{\int_v W(r,h) dv} \tag{2.8}$$

Equation (2.8) is derived by the same mass assumption of all particles and demonstrates that the fluid density is proportional to the particle number density.

2.2 Particles in MPS

2.2.1 Fluid particles

In order to simulate the flow in the MPS method, we need to use several different types of particles. Particles resulting from flow discretization are called Main particles or Fluid particles on which the Navier-Stokes equations are applied. As mentioned earlier, these particles carry various quantities such as pressure, density, temperature, mass, velocity, and so on. Since these particles are elements of the modeled fluid, wherever these particles are present, they indicate the presence of fluid in that area, and any property they carry with them indicates the property of the modeled fluid at that point. In specific cases, it is needed to identify the free-surface particles in order to assign the boundary values to them. In the standard MPS framework, the particle number density is being used for free-surface particle identification in which the criteria are met if the particle number density is less than a threshold:

$$n_i < \beta_n n_0 \tag{2.9}$$

In which the threshold factor β_n is between 0.8 and 0.99 (Shakibaeinia & Jin, 2010). Although this method is easy to implement, the more complex geometries need more accurate techniques (Marrone, Colagrossi, Le Touzé, & Graziani, 2010).

2.2.2 Wall particles

Wall particles (also called virtual particles) are among the first boundary particles and have been developed according to the initial applications of the MPS method. These particles are actually used to model the wall, and in some cases, they help to prevent the main particles from penetrating the wall by applying a strong impact force. This force is inversely proportional to the distance between the two particles, and when a fluid particle enters the area of influence of a virtual particle,

a force exerts in the direction of the center line of the particles and prevents them from approaching and penetrating into the boundary. One of the models to prevent particle penetration is as follows (G.-R. Liu & Liu, 2003):

$$F_{ij} = \begin{cases} D\left[\left(\frac{r_0}{r_{ij}}\right)^{n_1} - \left(\frac{r_0}{r_{ij}}\right)^{n_2}\right]\frac{x_{ij}}{r_{ij}^2} & \left(\frac{r_0}{r_{ij}}\right) \leq 1 \\ 0 & \left(\frac{r_0}{r_{ij}}\right) > 1 \end{cases} \tag{2.10}$$

In which the parameters n_1 and n_2 are considered 12 and 6, respectively. D is in the order of maximum speed in the problem, and r_0 is the range of effect of the virtual particles. This distance is usually the order of the initial distance between the particles. It should be noted that this repulsive force is not utilized in this research. The difference between these particles and the flow particles is that the Navier-Stokes equations are not solved for them, and in fact, their speed, location, Density, and pressure are constant and will not change. It is noteworthy that the necessity for the presence of another type of particle is noticeable since near the solid boundary, there is a kernel defect (Figure 2.1). As the virtual particles are stacked in only one row at the boundary, no particles are present on the other side of the boundary, and the boundary particle kernel near the walls is defective, causing an underestimation in the density of the boundary adjacent particles. This issue can be addressed with another type of particles, which are introduced below.

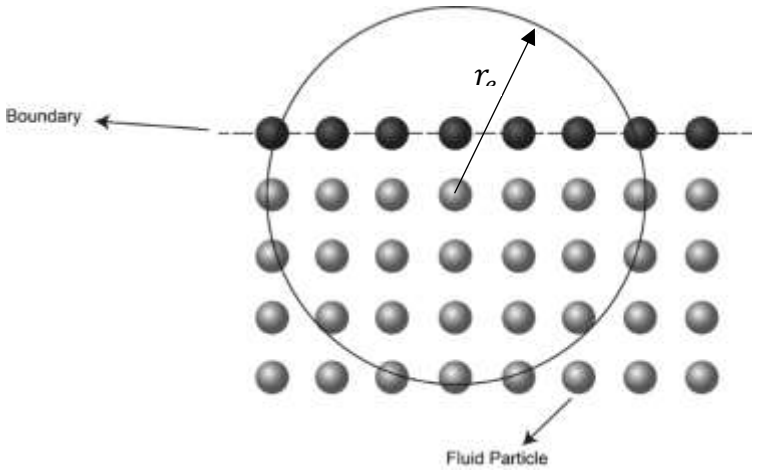

Figure 2.1 Wall particles and the deficiency of fluid particles' kernel near the boundary

2.2.3 Ghost Particles

Another type of particle that plays a crucial role in simulating using the MPS method is called the ghost particle. These particles have many tasks, including satisfying the non-slip boundary condition, preventing the penetration of particles, as well as repairing kernel defects for particles near the wall.

Since the velocity of the fluid must be zero at the stationary boundary (non-slip boundary condition), the behavior of the boundary particles must be such that the above condition satisfies. For this purpose, several rows of ghost particles are arranged symmetrically to the fluid particles with respect to the virtual (wall) particles (Figure 2.2). The velocities of these particles are symmetrical mirrors of the velocities of their respective fluid particles. This satisfies the condition of non-slip boundaries on virtual particles that actually act as solid boundaries. The non-penetration condition of the particles is also satisfied due to the position of the mirror particles in front of the fluid particle and the force exerted due to their presence.

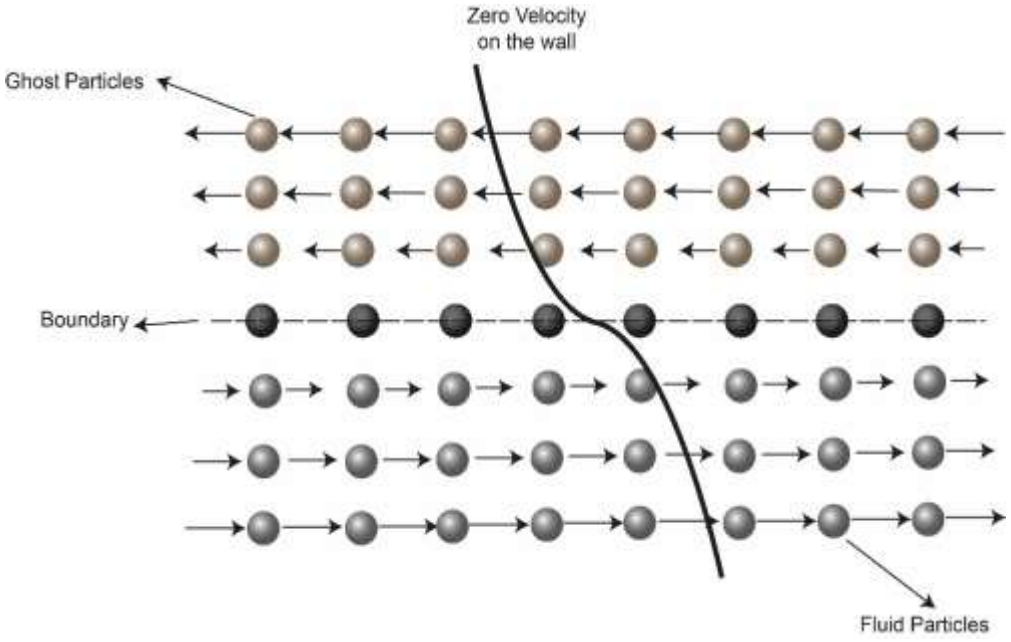

Figure 2.2 Ghost particles' impact on satisfaction of non-slippery boundary condition

As mentioned, the velocity components of the mirror particles are symmetrical to their corresponding fluid particles, but their density and pressure are the same as those of their corresponding fluid particles (Figure 2.3).

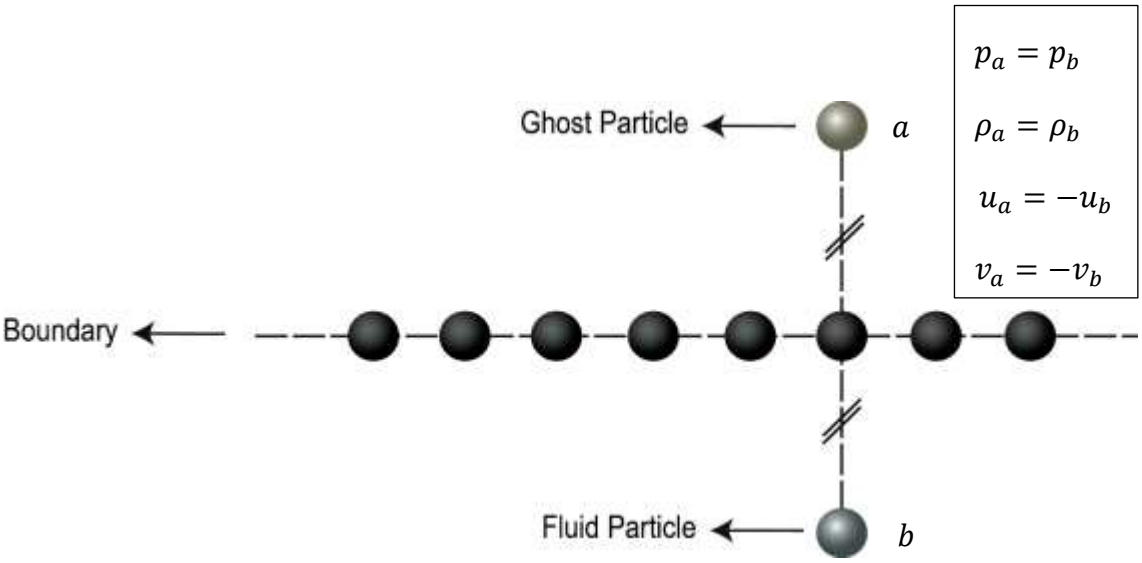

Figure 2.3 Mirror ghost particle

In addition, the number of rows of mirror particles is proportional to the radius of the fluid particle's kernel so that the kernel's deficiency will be solved. (Figure 2.4).

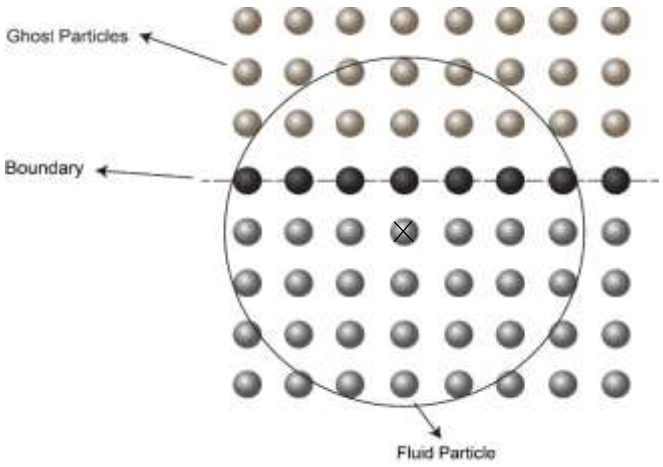

Figure 2.4 Solving the boundary particles' kernel deficiency using the ghost particles

In Figure 2.5, the representation of a physical domain in a continuum-based approach is depicted. It is notable that the ice floes and the water between them are considered as a single medium.

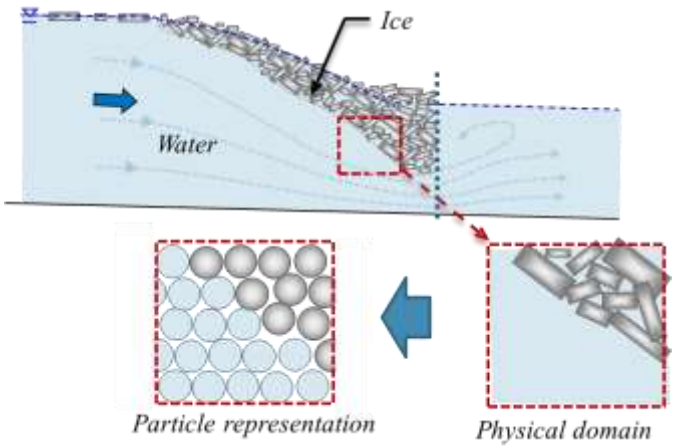

Figure 2.5 Particle-based representation of an ice-water system

2.3 Integral expression and particle approximation of a function

The MPS formulation is usually divided into two key steps. The first step is the integral expression or the kernel expression of functions and the second one is the particle approximation.

In the first part, integrating the multiplication of an arbitrary function and a kernel-smoothing function gives the kernel approximation of the function in the integral form. Then, the integral expression of the function is approximated by the sum of the values of the nearest neighboring particles, which leads to the approximation of the function particles at discrete points (particles).

The concept of integral expression of the function $f(x)$ used in MPS is derived from the following property:

$$f(x) = \int_{\Omega} f(x')\delta(x - x')dx' \tag{2.11}$$

In which $\delta(x - x')$ is the Dirac delta function which defines as:

$$\delta(x - x') = \begin{cases} 1 & x' = x \\ 0 & x' \neq x \end{cases} \tag{2.12}$$

In Equation (2.11) Ω is the integral volume that contains x. Due to the utilization of the Dirac delta function, the integral expression in Equation (2.11) is accurately expressed as long as the function $f(x')$ is defined and continuous in the range Ω.

By replacing the kernel function $W(x - x', h)$ with the Dirac delta function $\delta(x - x')$, the integral form of the function $f(x)$ is expressed as follows:

$$f(x) = \int_{\Omega} f(x')W(x - x', h)dx' \tag{2.13}$$

It should be noted that as long as W is not a Dirac function, the integral form expressed in Equation (2.13) can only be an approximation. Also in MPS, the kernel approximation operator is conventionally represented as follows:

$$\langle f(x) \rangle = \int_{\Omega} f(x')W(x - x', h)dx' \tag{2.14}$$

In the MPS method, the whole system is expressed by a limited number of particles, each of which has a specific mass and occupies a certain volume. This expression is obtained by particle approximation, which is another key operation in MPS and will be introduced later.

Continuous integral expressions using the smoothing function can be transformed into a discrete form of aggregation on all particles in their support domain. This disintegration and aggregation operation on particles is known as particle approximation in the MPS and SPH literature.

Substitute the very small volume dx' in the integral equation (2.14) at the particle j with the finite volume of the particle ΔV_j, which depends on the mass of the particle m_j as follows:

$$m_j = \Delta V_j \rho_j \tag{2.15}$$

Where ρ_j is the density of the particle j, which $j = (1,2,3, \dots, N)$ and N is the number of particles in the support area of the particle j.

With the given explanations, the continuous integral MPS form of the function $f(x)$ can be obtained in the discrete form of the following particle approximation.

$$(x) = \int_{\Omega} f(x')W(x - x', h)dx'$$

$$\cong \sum_{j=1}^{N} f(x_j)W(x - x_j, h)\Delta V_j \tag{2.16}$$

$$= \sum_{j=1}^{N} f(x_j)W(x - x_j, h)\frac{1}{\rho_j}(\rho_j \Delta V_j) = \sum_{j=1}^{N} f(x_j)W(x - x_j, h)\frac{1}{\rho_j}(m_j)$$

$$f(x) = \sum_{j=1}^{N} \frac{m_j}{\rho_j} f(x_j)W(x - x_j, h) \tag{2.17}$$

Equation (2.17) shows that the value of a function in particle j is approximated using the mean value of this function in the particles in the support range of that particle as it is weighted by the smoothing function.

2.4 Operators in the MPS framework

The governing equations that describe a physical phenomenon include mathematical operators such as derivatives, gradients, divergences, and Laplacian. Like other computational methods, these operators can be computed for the MPS method in the Lagrangian framework. The gradient operator in MPS can be expressed as:

$$\langle \nabla \phi \rangle_i = \frac{d}{n^0} \sum_{i \neq j} \frac{\phi}{|r_j - r_i|^2}(r_j - r_i)W(r_{ij}, h) \tag{2.18}$$

In which the n^0 is the particle number density far from the boundary and ϕ is an arbitrary scalar. The standard form of ϕ is:

$$\phi = \phi_i - \phi_j \tag{2.19}$$

Following, one can find the proposed values for the ϕ to calculate the pressure gradient:

$$\phi = \phi_i - \phi_{min,j} \quad \text{Koshizuka and Oka (1996)} \quad (2.20)$$

$$\phi = \phi_i + \phi_j \quad \text{Toyota et al (2005)} \quad (2.21)$$

$$\phi = \phi_i + \phi_j - \phi_{min,i} - \phi_{min,j} \quad \text{Khayyer \& Gotoh (2009)} \quad (2.22)$$

The divergence and Laplacian of a vector **u** can also be expressed as follows respectively:

$$\langle \nabla . \mathbf{u} \rangle_i = \frac{d}{n^0} \sum_{i \neq j} \frac{\mathbf{u}_j - \mathbf{u}_i}{|r_j - r_i|^2} . (r_j - r_i) W(r_{ij}, h) \quad (2.23)$$

$$\langle \nabla^2 \mathbf{u} \rangle_i = \frac{2d}{\lambda n^0} \sum_{i \neq j} (\mathbf{u}_j - \mathbf{u}_i) W(r_{ij}, h) \quad (2.24)$$

The parameter λ in the Laplacian is a correction parameter that keeps the variance increasing (Koshizuka & Oka, 1996) and is defined as:

$$\lambda = \frac{\int_V W(r_{ij}, h) r^2 dv}{\int_V W(r_{ij}, h) dv} \quad (2.25)$$

2.5 Calculating pressure

The pressure is calculated using the Poisson equation in the original form. In 2010, Shakibaeinia and Jin (Shakibaeinia & Jin, 2010) Proposed a modified form of weakly compressible treatment for the MPS pressure calculation which was developed for the SPH method by Monaghan (J. J. Monaghan, 1994). In this approach, the flow is considered nearly incompressible, so the pressure can be explicitly calculated for each particle. The Modified Tait's equation for the MPS is expressed is:

$$P_i^{n+1} = \frac{\rho_i c_0^2}{\gamma}(((\mathrm{n}^*\rangle_i/n^0)^\gamma - 1) \tag{2.26}$$

In which the c_0 is the numerical sound speed and is usually set to be more than 10 times the maximum speed of the flow field to satisfy the compressibility ratio remaining under 1%.

2.6 Simulation Enhancements

Due to the nature of particle methods, using particle rearrangement techniques is inevitable. These regularization techniques are common methods to improve the particle distributions in order to avoid particle clustering and density fluctuations. The pair-wise particle collision (PC) method is one of the approaches which is widely used in the WC-MPS method (Shakibaeinia & Jin, 2012). In this method, the velocity vector of the particles whose distance is less than a threshold will be decomposed into normal and tangential parts. The assumption in this method is that the tangential part is negligible and only the normal part will be affected and corrected. The other method to enhance the models accuracy is the corrected particle shifting method developed by Jandaghian and Shakibaeinia (M Jandaghian & Shakibaeinia, 2020) which the idea is taken from "Fick's law of diffusion" implemented by Linda et al. (Lind et al., 2012). In this method, the particles are shifted from higher particle concentration regions to lower ones. The XSPH method (J. Monaghan, 1989) can also be mentioned as another regularization technique to avoid the inter-penetration of particles. This method affects the velocity of particles based on the average velocity of the neighbor particles.

2.7 Solution algorithm

In this study, the governing equations are solved using a fractional step method which splits the time steps into prediction and correction pseudo steps. The velocity of a particular particle can be obtained by the summation of the velocity calculated in the prediction and correction steps (Shakibaeinia & Jin, 2012).

$$u_i^{k+1} = u_i^* + u_i' \tag{2.27}$$

In which the $*$ and $'$ superscripts denote the prediction and correction steps respectively. The predicted velocity can be calculated as follows:

$$\begin{aligned} u_i^* &= u_i^k + \Delta \mathrm{u}_i^* \\ \Delta \mathrm{u}_i^* &= \frac{\Delta t}{\rho_i}(f_i + \nabla \mu_i(\nabla . \mathbf{u}_i) + \mu_{ij}\nabla^2 \mathbf{u}_i \end{aligned} \tag{2.28}$$

By calculating the predicted velocity we can simply move the particles accordingly in the prediction step:

$$r_i^* = r_i + u_i^* \Delta \mathrm{t} \tag{2.29}$$

After predicting the position of particles, the new particle number density will be calculated. The difference between initial and predicted particle number density can be utilized to calculate the pressure. The correction step of the velocity is as follows:

$$u' = -\frac{\Delta t}{\rho_i}\nabla p_i \tag{2.30}$$

As it has already been mentioned, the velocity in the new time step can now be calculated by the summation of predicted and corrected steps.

The algorithm of the MPS method can be represented by the following flowchart:

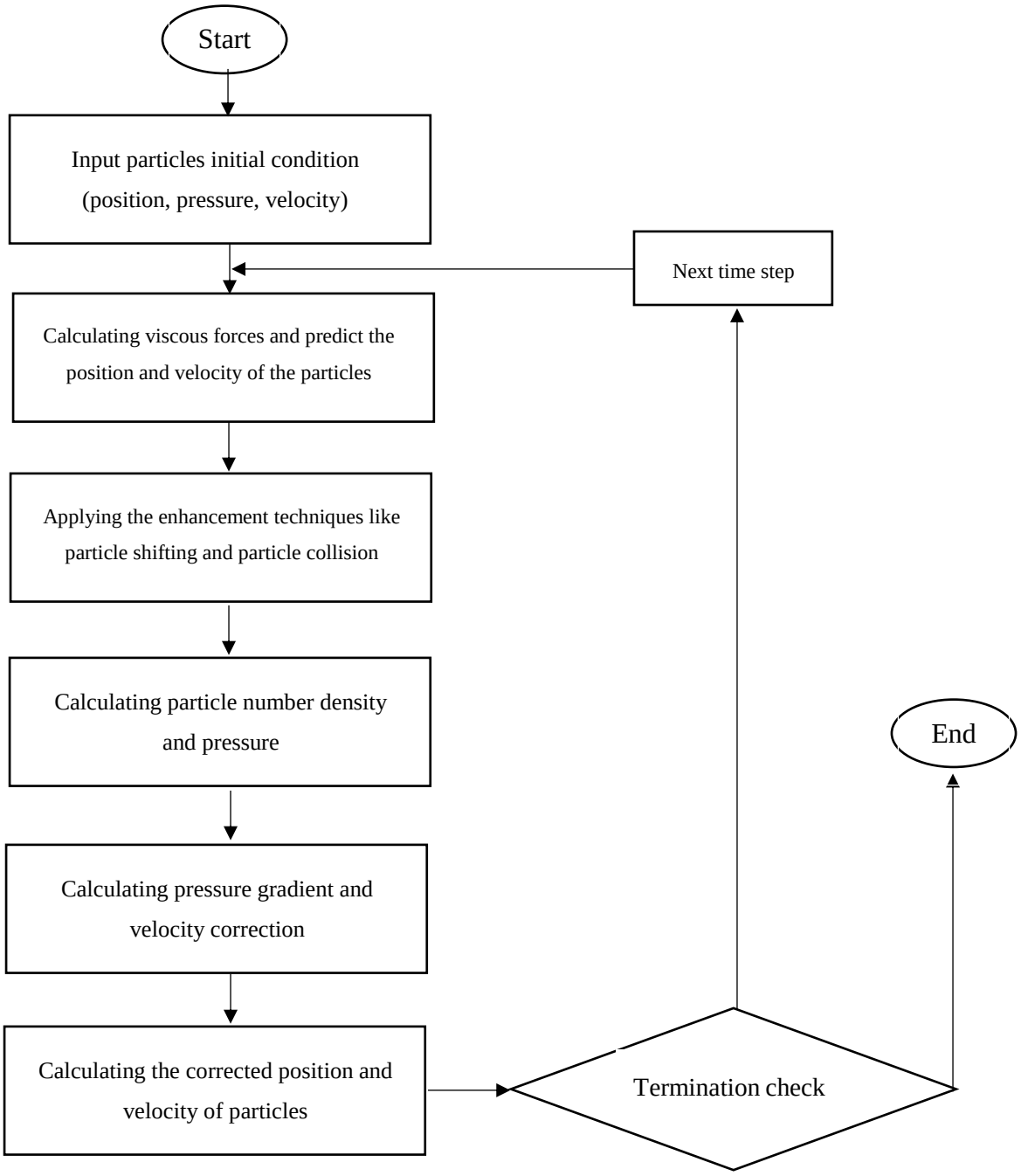

Figure 2.6 MPS algorithm flowchart

2.8 Time step calculation

As the described time integration scheme solves the weakly compressible fluid flows explicitly, the CFL condition should be satisfied in computing the time step (A. J. Crespo et al., 2015). We implement this condition as follows:

$$\Delta t \leq C_{CFL} \frac{l_0}{c_0} \tag{2.31}$$

In which C_{CFL} is the courant number which is between 0 and 1 (Shakibaeinia & Jin, 2010). Since in this study the shear stress is dominant the time step will be calculated as follows (Violeau & Leroy, 2014):

$$\Delta t = \min\left\{C_{CFL} \frac{l_0}{c_0}, 0.125 \frac{\rho_m l_0^2}{\eta_{max}}\right\} \tag{2.32}$$

In which the η_{max} is the maximum viscosity of the system.

Chapter 3 RHEOLOGICAL MODELS

In the event of a dam break, simulating the rise in water level and discharge is important for public safety. For instance, in Canada, the owner is legally obliged to conduct hydrodynamic studies using numerical models to determine the increase of water and the speed of surge for different dam break scenarios (According to Centre d'Expertise Hydrique du Québec 2007). Since most of the North American rivers are frozen during the winter, and the fact that the resulting ice floes in spring can accumulate and act as a dam, understanding and simulating this so-called ice jam phenomenon is of high importance, especially for cold regions. For this reason, this study aims to investigate the ability of particle-based methods, namely MPS, with a continuum approach and its capabilities to couple with rheological models, Standard Visco-Plastic (SVP) and Herschel-Bulkley-Papanastasiou (HBP), to simulate the ice dynamics and its interactions with fluids. Two experimental test cases namely ice jamming formation conducted at the university of Alberta (Healy & Hicks, 2006) and laboratory scale punch-through test (Polojärvi, Tuhkuri, & Korkalo, 2012) are simulated and the results are compared and validated.

3.1 Rheological models

In the continuum-based simulations of ice-fluid models, the rheology of the non-Newtonian phase plays a crucial role. In fact, in non-Newtonian fluids, there is no linear relationship between shear stress and shear rate. Starch suspensions, many salt solutions, and toothpaste are all considered non-Newtonian fluids. The rheological model is a link between ice internal stress, deformation, and mechanical strength. The well-known Standard Visco-Plastic (SVP) rheological model is currently being used in most ice dynamic models thanks to its simplicity in numerical simulation implementations on large scales and relatively acceptable results. Also, as early studies show, river ice can be considered a granular material with bulk rheology. Hence, the Herschel-Bulkley (HB) model which is mostly used for granular materials is also investigated for the sake of comparison.

For an arbitrary tensor $\mathbb{A}$, the standard definitions in tensor calculus are such that the trace is given by $tr(\mathbb{A})$, $\mathbb{A}^T$ is the transpose of $\mathbb{A}$, the first and second invariants are I_A and II_A, the magnitude is defined by $\|A\| = \sqrt{II_A} = \sqrt{0.5\ \mathbb{A} : \mathbb{A}}$ and $\mathbb{A}' = \mathbb{A} - \frac{1}{D} tr(\mathbb{A})\mathbb{I}$ is the deviator in which D is the

number of spatial dimensions and $\mathbb{I}$ is the unit tensor. For a general viscous compressible fluid, the total stress tensor can be defined as:

$$\mathbb{T} = \tau - P\mathbb{I} \tag{3.1}$$

In which:

$$\tau = 2\eta\mathbb{E} + \zeta(\nabla.\boldsymbol{u})\mathbb{I} \tag{3.2}$$

In the above equation, τ is the shear stress tensor,η is the effective viscosity, $\mathbb{E} = 0.5(\nabla\boldsymbol{u} + (\nabla\boldsymbol{u})^T)$ is the strain rate tensor and ζ is the second coefficient of viscosity representing a combination of all the viscous effects associated with the volumetric rate-of-strain (Nodoushan et al., 2018).

For the ice phase, the effective viscosity is $\eta = \eta(\|\mathbb{E}'\|, P')$ in which $\mathbb{E}'$ is the deviator of the strain rate tensor and P' is the mechanical pressure or normal stress. The rheological model defines the effective viscosity with some relations which are dependent on the non-Newtonian material which is ice in this study.

3.1.1 HB model

The Herschel-Bulkley (HB) generalized visco-plastic has been widely used for modeling granular flows (Huang & Garcia, 1998) and is being evaluated in this study for modeling ice dynamics. This model considers the material as a rigid body for stresses less than yield stress and as a viscous fluid for stresses more than this yield stress. The stress tensor in the Herschel-Bulkley (HB) model is defined as:

$$\mathbb{T} = 2\eta\mathbb{E}' - P\mathbb{I} \tag{3.3}$$

The effective viscosity of the HB model is as follows (Nodoushan et al., 2018):

$$\eta = \begin{cases} \dfrac{\tau_y}{2\|\mathbb{E}'\|} + \eta_0(\|\mathbb{E}'\|)^{\beta-1} & \|\tau\| > \tau_y \\ \eta_{max} & \|\tau\| \le \tau_y \end{cases} \tag{3.4}$$

In which η_0 and β is the flow consistency and behavior indices which are typically determined through rheometry measurements and are dependent on the material properties. The HB model also accounts for the post-failure behavior of the stress tensor. Where the shear rate approaches zero ($\|\mathbb{E}'\| \rightarrow 0$; $\|\tau\| \rightarrow \|\tau_y\|$), equation (3.4) is discontinuous and singular for the un-yielded flow regions. To overcome this singularity, a popular exponential regularization continuous version of the equation proposed by Papanastasiou (Papanastasiou, 1987) is utilized as follows:

$$\eta = \frac{\tau_y(1 - \exp(-m\|\mathbb{E}'\|)}{2\|\mathbb{E}'\|} + \eta_0(\|\mathbb{E}'\|)^{\beta-1} \tag{3.5}$$

In which parameter m controls the exponential growth of stress such that by increasing the m, the shear stress will get closer to the ideal one (equation (3.4)) as shown in Figure 3.1. The regularized equation is valid for both yielded and un-yielded regions.

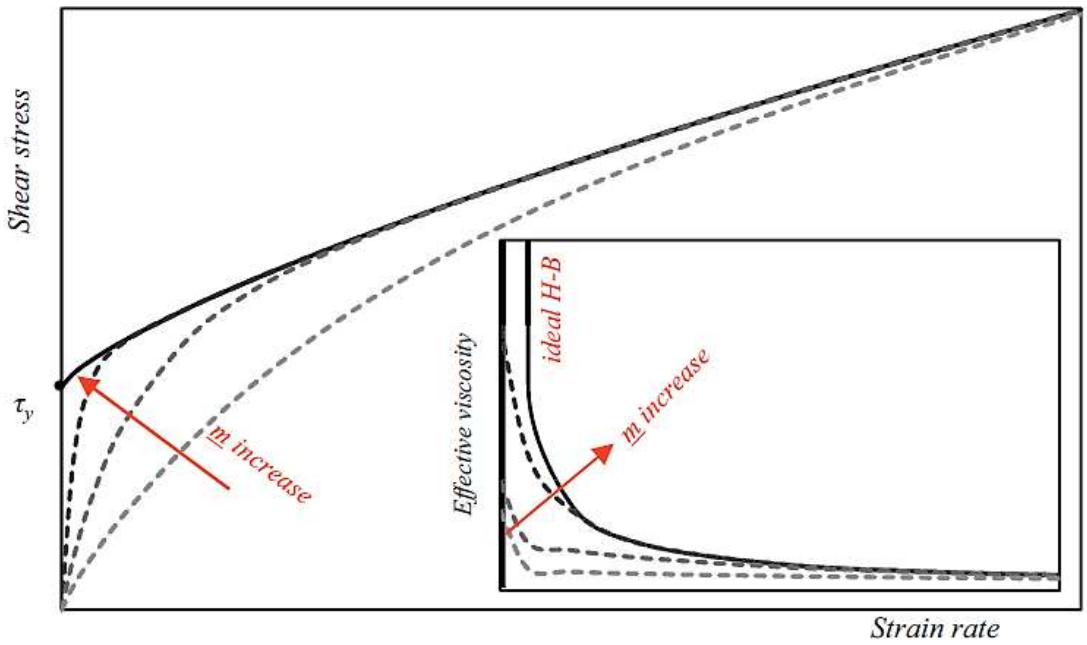

Figure 3.1 Schematic of shear stress and viscosity variation for exponential regularized HB model (Nodoushan et al., 2018)

For the un-yielded regions, the effective viscosity has a maximum of $\eta_{max} = \eta_0 + 0.5m\tau_y$ which is a function of yield stress and normal stress.

3.1.2 Standard viscous-plastic model (SVP)

The standard Visco-Plastic rheological model proposed by Hibler (Hibler III, 1979) which is commonly used for large dimension ice dynamic-related problems in the literature is implemented in this study. This model is patterned after the AIDJEX model developed by Coon et al. (Coon et al., 1974). The SVP constitutive law is not as detailed as the AIDJEX model and it is much more practical which allows larger time steps.

The studies associated with the AIDJEX program revealed that rate-independent plastic rheologies are most appropriate for sea ice dynamic interactions. The idea behind these plastic rheologies is to allow having the equivalent stresses in the ice pack for the small as well as the large deformation rates. However, in linear viscous rheologies, the stresses are proportional to the deformation rate (See Figure 3.2). Moreover, these rheologies are strongly resistance to compressive and shearing deformations whereas they allow dilation to happen with almost no stress.

To model the plastic behavior, the ice was considered as an elastic-plastic continuum in which the ice behaves elastically in certain strain states. Though, the inclusion of the elasticity demands keeping track of the strain state of a given portion of ice indefinitely which introduces significant mathematical complexity both theoretically (Pritchard, 1975) and numerically (Colony, Pritchard, & Pritchard, 1975).

To overcome the complexity problem and retain the plastic behavior at the same time, Hibler et al (Hibler III, 1979) considered the sea ice as a nonlinear viscous compressible fluid. In this approach, the nonlinear viscosities are treated differently for normal and very small deformation rates. For normal deformation rates, the ice interacts in a rigid-plastic manner and for very small deformation rates, it is treated as a linear viscous fluid with a pressure term. This viscous-plastic approach even helps the Eulerian formulations by modeling the essential features of a plastic fluid without time step limitations by using implicit numerical techniques.

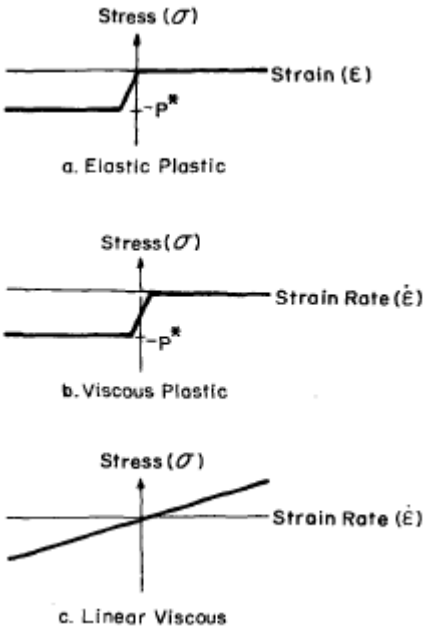

Figure 3.2 One-dimensinal comparison of elastic-plastic, viscous-plastic and linear viscous rheologies (Hibler III, 1979)

Figure 3.2 illustrates a comparison between the present viscous-plastic approach, the elastic-plastic method, and linear viscosity in one dimension. Regarding the elastic-plastic case, one can perceive that the material resists compression with a fixed stress and has no resistance to diverging strains. The same trend can be found in the viscous-plastic case except that the stress is related to the magnitude of the strain rate instead of the strain itself. An important difference between these two plastic laws is in the treatment of relatively motionless situations. In the elastic-plastic model, by allowing the ice to behave elastically, high stress can be maintained without any relative ice motion. In the visco-plastic case, however, such “rigid” cases are approximated by a state of creeping flow. A significant difference between the linear viscosity and plastic approaches is that even for small strain rates, the stresses are large and independent of the rate of deformation.

3.1.2.1 SVP constitutive law

As already mentioned, for modeling the ice interaction in the visco-plastic approach, the ice is considered to be a nonlinear viscous compressible fluid that obeys the following stress tensor:

$$\mathbb{T} = 2\eta\mathbb{E}' - P\mathbb{I} + \left(\frac{P}{2} + \zeta E_I\right)\mathbb{I} \tag{3.6}$$

In which $\mathbb{I}$ is the identity tensor, $\mathbb{T}$ is the stress tensor (two-dimensional), $\mathbb{E}'$ is the deviatoric strain rate tensor, P is a pressure term and ζ and η are nonlinear bulk and shear viscosities. The pressure term (yield strength in isotropic compression) is suggested to be parametrized by the following equation (J. F. Lemieux & Tremblay, 2009):

$$P = P^* hexp(-C(1-A)] \tag{3.7}$$

In which P^* is the ice strength per meter, A is sea ice concentration and C is an empirical constant characterizing the dependence of the compressive strength on sea ice concentration. However, in our weakly compressible model, the pressure is calculated using the equation of state.

The bulk and shear viscosity define the rheology term which depends on the yield curve and the flow rule. As suggested by Hibler, the elliptical yield curve with a normal flow rule is used for the standard visco-plastic model. In this case, the bulk and shear viscosities are defined as follows:

$$\zeta = \frac{P}{2\Delta} \tag{3.8}$$

$$\eta = \zeta e^{-2} \tag{3.9}$$

In which:

$$\Delta = \sqrt{E_I^2 + \left(\frac{E_{II}^2}{e}\right)^2} \tag{3.10}$$

In the above equation, e is the ratio of the long axis and the short axis of the elliptical curve (Figure 3.3)

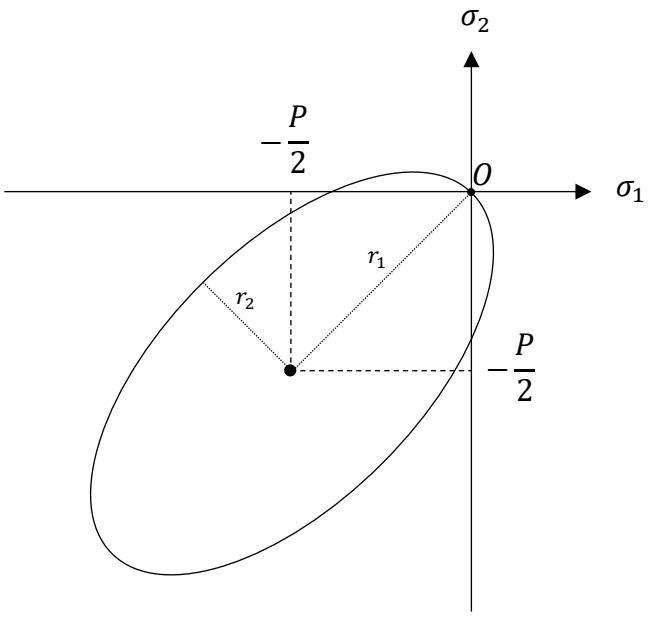

Figure 3.3 Elliptical yield curve of standard viscos plastic rheology with $e = \frac{r_1}{r_2} = 2$

Figure 3.3 shows the relationship between the two-dimensional principal components of stress (σ_1 and σ_2) of a visco-plastic rheology that employs an elliptical yield curve. The elliptical curve boundary shows the plastic flow which the stress state lies on it and its location is specified by the strain rate principal components.

When Δ tends to zero, equations (3.8) and (3.9) tend to infinity and become singular. Hibler (Hibler III, 1979) proposed a maximum value of $\zeta_{max} = (2.5 \times 10^8)P$ and $\eta_{max} = \zeta_{max} e^{-2}$ and also in order to avoid potential instabilities their minimums are also limited by $\zeta_{min} = (4 \times 10^8) kgs^{-1}$ and $\eta_{min} = \zeta_{min} e^{-2}$. Hence the equations (3.8) and (3.9) will be like:

$$\zeta = \max\left(min\left(\frac{P}{2\Delta}, \zeta_{max}\right), \zeta_{min}\right) \tag{3.11}$$

$$\eta = \max\left(min\left(\frac{P}{2e^2\Delta}, \eta_{max}\right), \eta_{min}\right) \tag{3.12}$$

This formulation of the viscous coefficients with capping leads to a rheology term that is not continuously differentiable with respect to the velocity. To obtain a smooth formulation of the

viscous coefficients, Lemieux and Tremblay (J. F. Lemieux & Tremblay, 2009) have proposed the following:

$$\zeta = \zeta_{max} \tanh\left(\frac{p}{2\Delta\zeta max}\right) \tag{3.13}$$

Lemieux and Tremblay (J. F. Lemieux & Tremblay, 2009) have shown that this smooth formulation reduces the number of OL iterations required to reach full convergence by a factor of ~ 2 with the standard solver.

Chapter 4 RESULTS AND DISCUSIONS

In this chapter, the simulation and the evaluation of two test cases, namely Punch through and ice jam, are done using the developed model. To do so, the ice floes and the water particles between them are considered as a single phase which their properties are reflected in their rheological models.

4.1 Punch through simulation

For the sake of validation, an experiment of punch through test (Polojärvi et al., 2012) is examined here with our developed continuum-based MPS method. In this experiment laboratory-scale punch-through tests are done using the plastic blocks (rubbles) acting as ice. Their motivation for using plastic blocks instead of ice was to simplify the interpretation of results, as they won't freeze like real ice while they are together. Comparisons are done to validate the authenticity of the results.

4.1.1 Problem definition

The punch-through test conducted by Poljärvi et al (Polojärvi et al., 2012) was in two types: uncovered and covered basins. These types differed by the boundary conditions on the top of the rubbles. Figure 4.1 shows the experimental setup in which y_I is the direction of the indenter's motion. The basin covers as well as the rubbles are not shown in Figure 4.1 for the sake of clarity. Table 4.1 shows some of the parameters used in this experiment.

Table 4.1 Parameters in the punch-through experiment

PARAMETER	VALUE
NUMBER OF BLOCKS	$1450 - 3800$
GRAVITATIONAL ACCELERATION	$9.8\ m/s^2$
BLOCK LENGTH	$0.09\ m$
BLOCK WIDTH	$0.05\ m$
BLOCK THICKNESS	$0.02\ m$
MASS DENSITY	$949\ kg/m^3$
INDENTER'S THICKNESS	$0.01\ m$

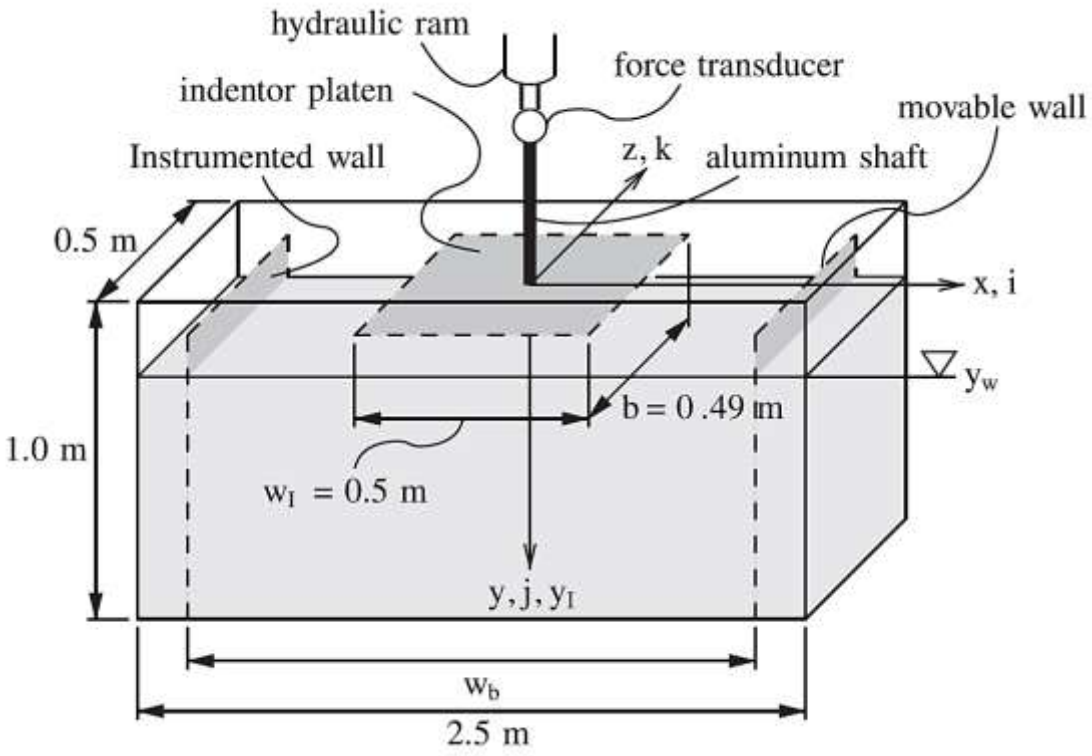

Figure 4.1 Experimental setup (Polojärvi et al., 2012)

The W_b is the instrumented wall width which is movable in their experiment but here we have fixed walls with $2.5\ m$ widths.

The position of the initial particles of punch through test with lid are as shown in Figure 4.2. The total number of particles is around 20k in these simulations including the fluid, boundary, and ghost particles. In Table 4.2, more detailed parameters used in this simulation can be found. For the indenter, only one layer of the solid particle is used which ensures the maximum pressure validity in the flow field. In the simulations conducted in this research, the indenter's speed is $10\ mm/s$. For the ice phase, both rheological models, namely SVP and HB are applied and examined.

Table 4.2 Parameters used in the punch through simulation

PARAMETER	**VALUE**
NUMBER OF FLUID PARTICLES	19200
NUMBER OF BOUNDARY PARTICLES	600
NUMBER OF GHOST PARTICLES	1800
AVERAGE PARTICLE DISTANCE	0.01 m
SUPPORT AREA RADIUS	0.031 m
KERNEL FUNCTION	$Rational\ function$
SPEED OF SOUND	30 m/s
WATER'S DENSITY	1000 kg/m^3
ICE'S DENSITY	950 kg/m^3

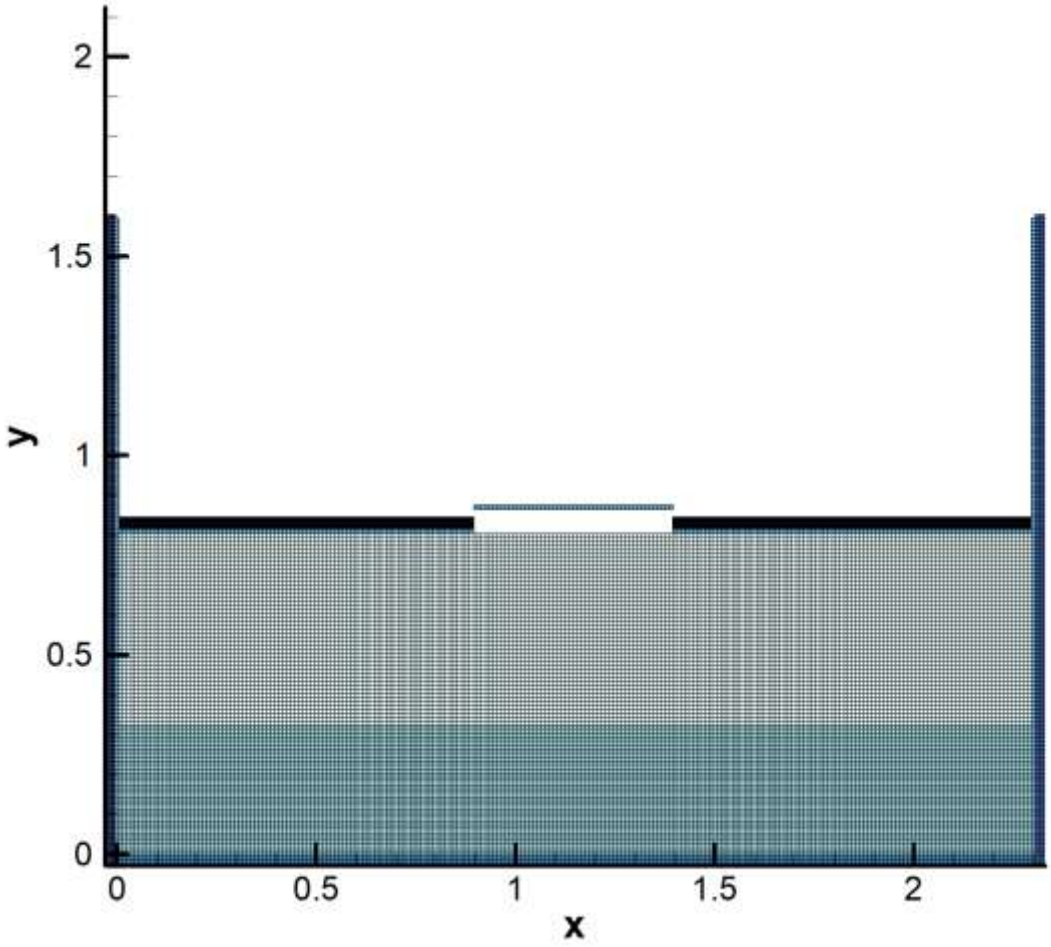

Figure 4.2 initial condition of punch through test with lid

4.1.2 Results and analysis

By moving the indenter toward the tank, the ice medium will start to interact with it. Due to the viscosity of the ice phase, the border of their particles with the water phase will have a formation at each level of the indenter's penetration. The particles' formation are shown in two different levels in Figure 4.3 and the borders are compared in Figure 4.4 and Figure 4.5. It should be noted that there was no major difference in particle formation for the two examined rheological models.

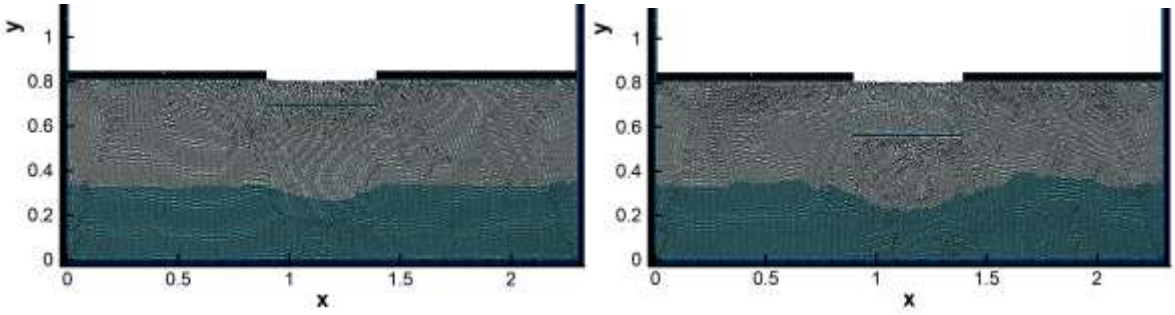

Figure 4.3 Position of ice and water particles in $y_i = 80\ mm$ and $y_i = 240\ mm$

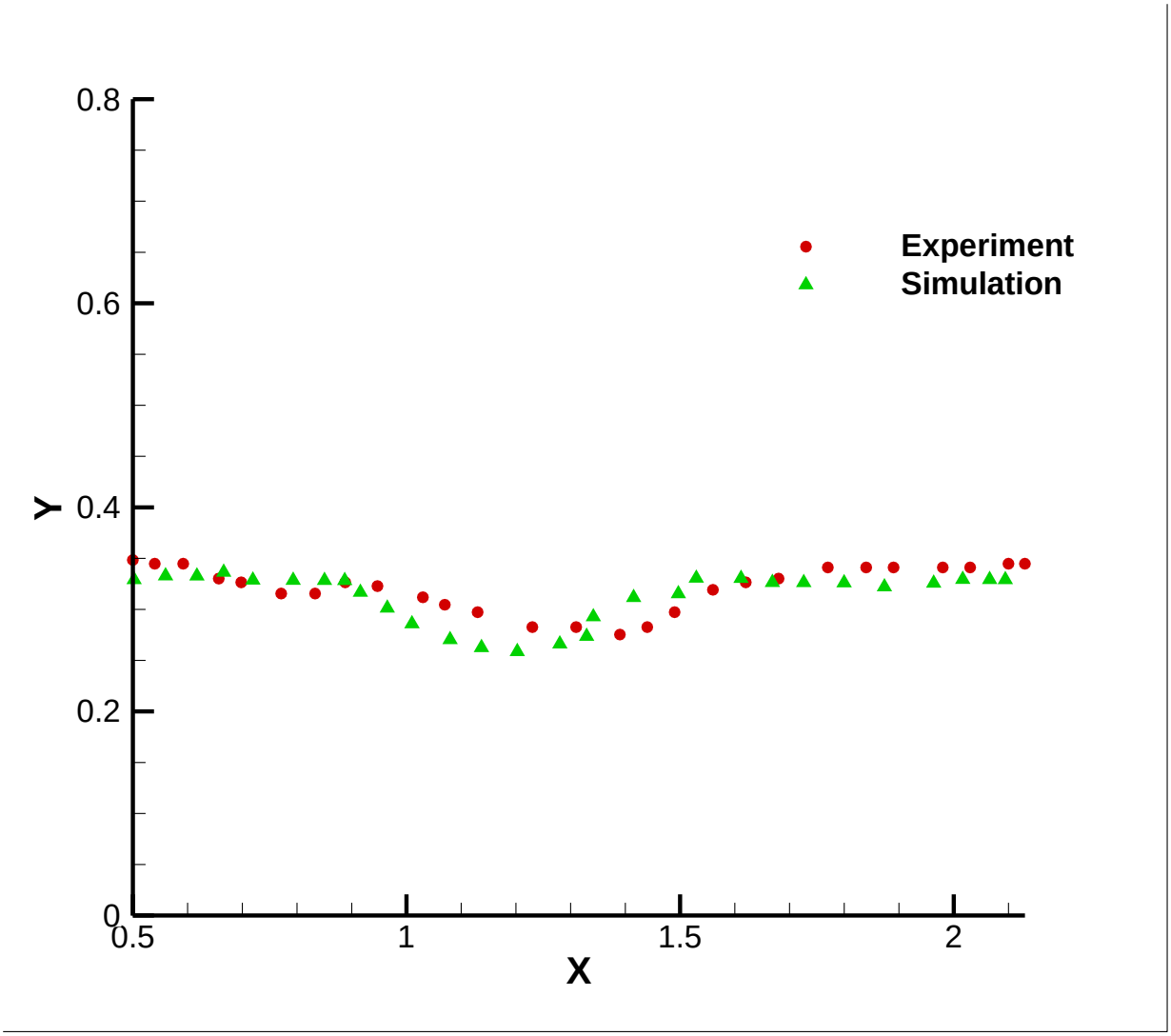

Figure 4.4 Ice medium border comparison with the experimental results in $y_i = 80\ mm$

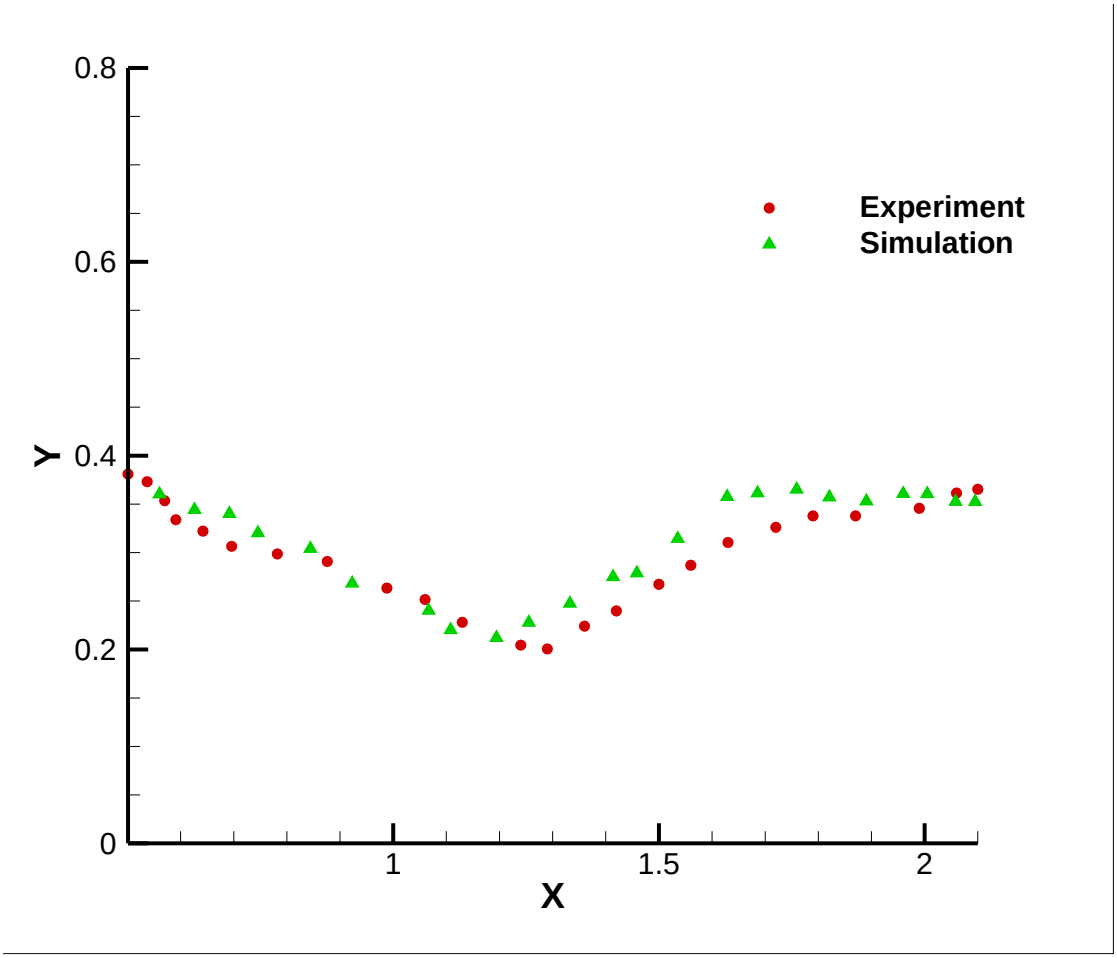

Figure 4.5 Ice medium border comparison with the experimental results in $y_i = 240\ mm$

The comparison of the borders of the ice medium between the experimental result and the developed model shows good agreement, which in turn can be an indicator of an authentic estimation of viscosity. Figure 4.6 shows the contour of the logarithm of viscosity in $y_i = 240\ mm$. The viscosity near the walls and under the indenter is higher due to the increment of normal stress.

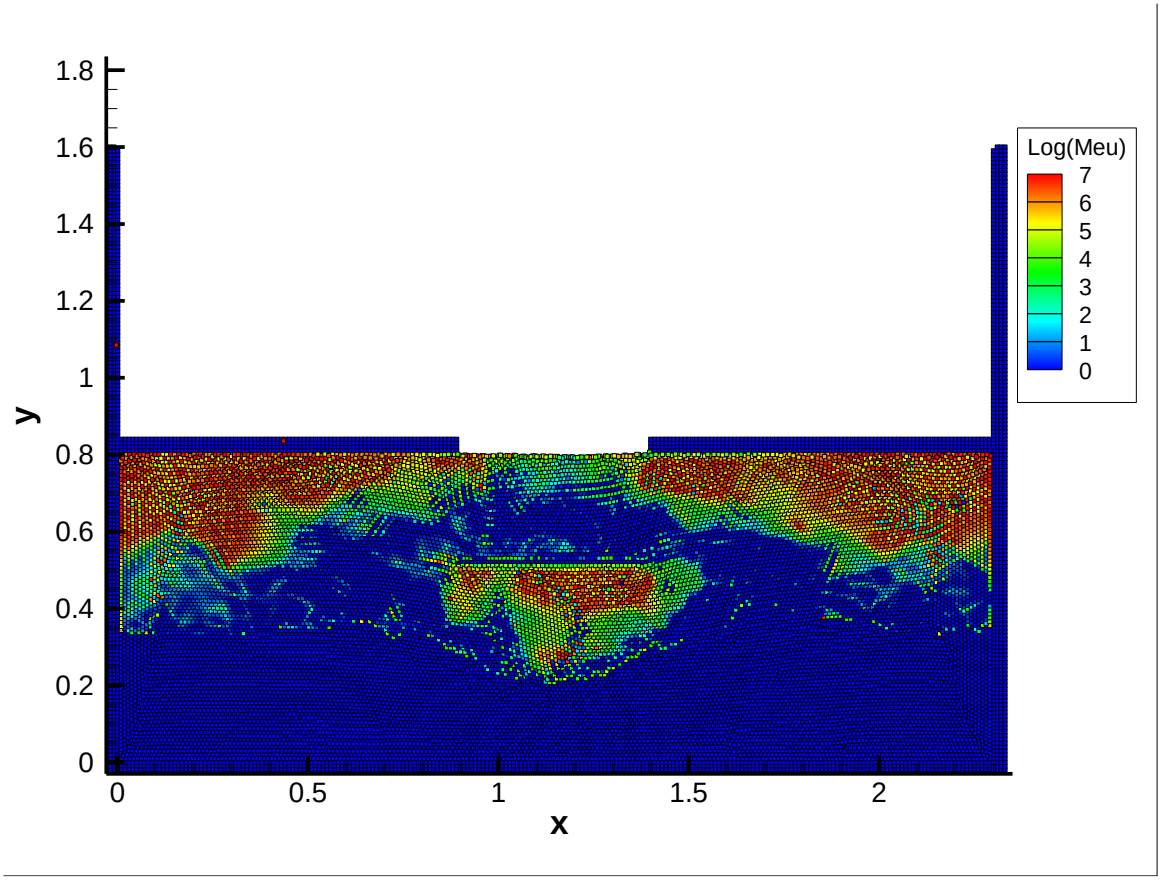

Figure 4.6 The logarithm of viscosity in $y_i = 240\ mm$

To examine more the validity of the developed model, the ratio of vertical displacement of particles to the indenter's displacement is shown in a contour and is compared with the experimental results. The margins provided for the experimental results for different ratios are approximate since the contour is not provided. However, the depicted contour of the developed model shows the particles with different ratios of displacement with respect to the indenter's displacement.

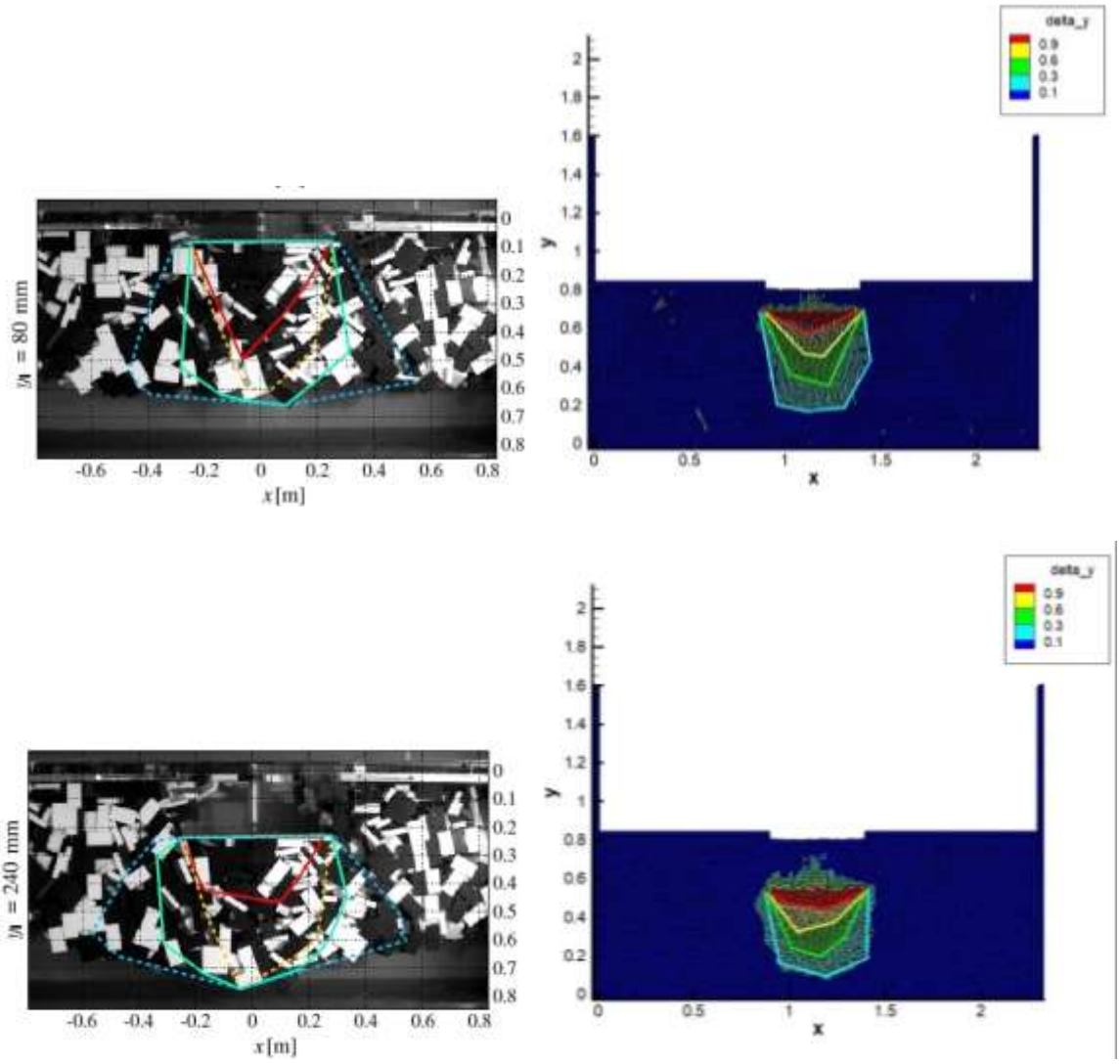

Figure 4.7 Deformation of particles based on the ratio to the indenter's displacement. Left: experimental results, Right: numerical results.

Finally, in order to examine the accuracy of rheological models in this test case, the volume of displaced particles with different vertical velocities is traced while the indenter penetrates the tank (Figure 4.8). It should be noted that the experimental results are approximate and are an average of repeated experiments.

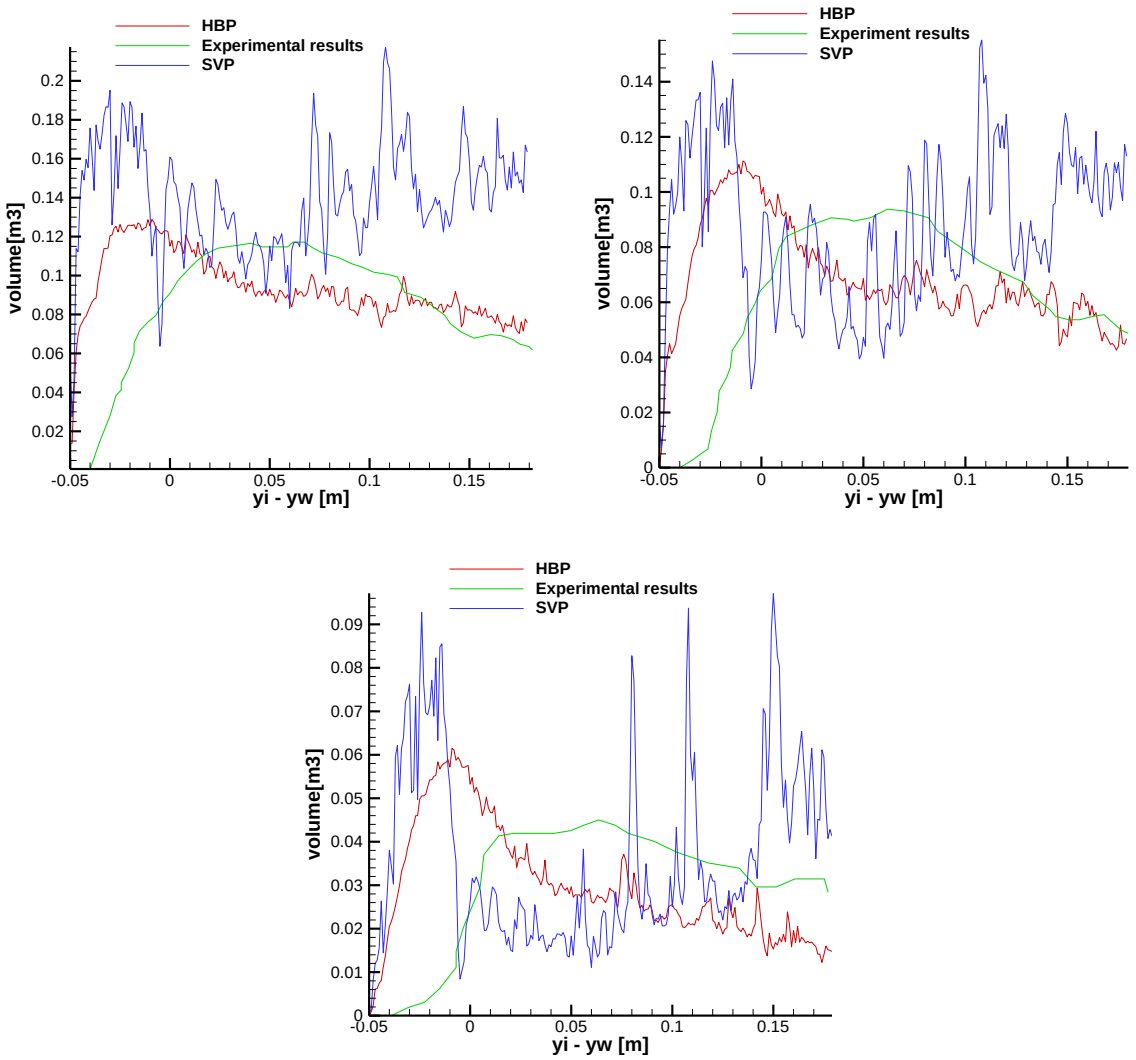

Figure 4.8 Volume of displaced ice particles with three vertical velocities v_y=2,5 and 9 mm/s

The results obtained in Figure 4.8 shows relatively good agreement with the experimental results. As the experimental results are not unique and can be lightly varied by changing the conditions of the experiment, the developed model results are valid as long as they follow the trend and magnitude. However, the Herschel-Bulkley model seems to follow the trend more accurately. It should be noted that the experimental results presented in Figure 4.8 are the average of many repeated experiments as shown in Figure 4.9. The reason for fluctuations in the results of the developed model can be related to the nature of particle-based methods. Since the volume of displaced particles are proportional to the number of them (The volume of particles is constant

during the simulation), the quantity of particles meeting the velocity criteria varies at each time step.

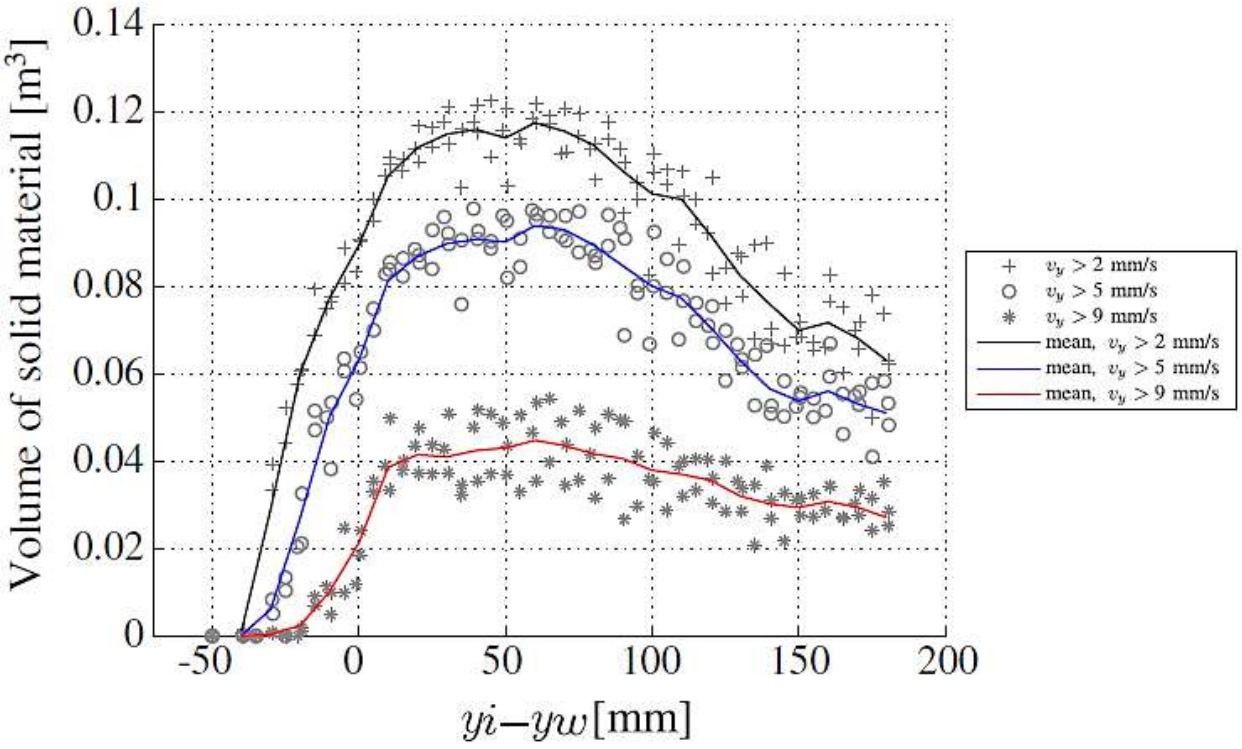

Figure 4.9 Numerical results of volume of displaced ice particles (Polojärvi et al., 2012)

In addition to the fluctuation of the results, there are some discrepancies between the actual experiment and the simulation that affect the accuracy of the results. Having a closer look at the beginning of the indenter's movement, the reason for not perfectly matched results can origin from different thicknesses of the indenter in the simulation from the experiment. Also, the 3D effects are not taken into account which can definitely affect the results.

4.2 Ice jam simulation

4.2.1 Problem definition

A more dynamic and larger-scale case is simulated in this part. The developed model is applied and validated for a case of ice jam formation based on the experiments of (Healy & Hicks, 2006). The experiments were carried out in $32m$ long, $0.91m$ high sidewalls and $1.22m$ width recirculating flume. Some of the parameters used in this experiment are presented in Table 4.3.

Table 4.3 Parameters used in Ice jam experiment

PARAMETER	VALUE
MODEL ICE FLOW SIZE	$varies\ from$ 1.27 to 5.08 $cm\ on\ each\ dimension$
GRAVITATIONAL ACCELERATION	9.8 m/s^2
ICE & WATER DISCHARGE RATE	35 L/s $-$ 65 L/s
FLOATING POLYWOOD SIZE	$1.9cm \times 1.22m \times 1.22m$
FLUME'S LENGTH	32 m
FLUME'S HEIGHT	0.91 m
FLUME'S WIDTH	1.22 m

A sheet of plywood is positioned at $24m$ downstream of the flow to simulate an intact ice cover and initiate the ice jamming. For this test, discharges of $34 - 48\ L/s$ are supplied to the head tank (Figure 4.10). The experiments are done with and without a wire mesh to block the ice parcels and initiate the ice jamming. This test case is simulated using approximately 21k particles for the initial condition and this number goes up to 26k during the simulation. Some of the parameters used in this simulation can be found in Table 4.4.

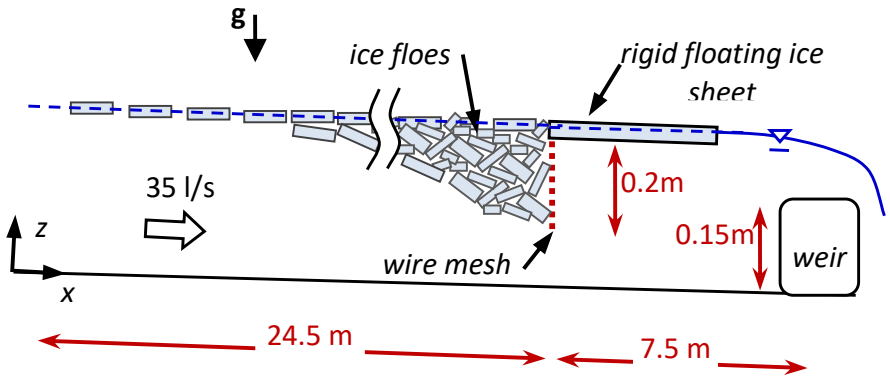

Figure 4.10 Ice jam experimental setup schematic

Table 4.4 Parameters used in ice jam's simulation

PARAMETER	VALUE
NUMBER OF FLUID PARTICLES	$14k - 19k$
NUMBER OF BOUNDARY PARTICLES	1650
NUMBER OF GHOST PARTICLES	4950
AVERAGE PARTICLE DISTANCE	0.02 m
SUPPORT AREA RADIUS	0.062 m
KERNEL FUNCTION	$Rational\ function$
SPEED OF SOUND	25 m/s
WATER'S DENSITY	1000 kg/m^3
ICE'S DENSITY	950 kg/m^3

4.2.2 Boundary treatment

One of the challenges in this test case was dealing with the inlet and outlet of the flume as the inflow and outflow are different which needs generation and elimination of the particles. If the particles suddenly appear in the inflow, the sudden increase of the particle number density will introduce an unphysical pressure to the flow domain which causes unphysical acceleration to the inflow particles. To tackle this issue, the approach introduced by (Shakibaeinia & Jin, 2011) is implemented in which layers of ghost particles are set in the inflow with the same velocity and pressure of the inflow particles (Figure 4.11). New generated particles appear in the last layer of ghost particles and move toward the flow field. By this trick, the unphysical pressure problem can be handled.

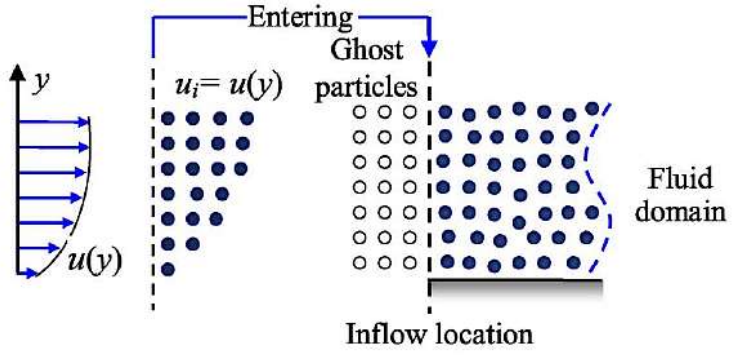

Figure 4.11 Inflow particle generation treatment (Shakibaeinia & Jin, 2011)

For the outflow, however, adding layers of ghost particles seems not to be enough to compensate for the lack of particle number density. As it is shown in Figure 4.12, when a particle is removed, the particles in its support domain will instantly be affected and their particle number density and in turn their pressure will drop significantly, which is not an ideal thing. The layers of ghost particles can gradually compensate for this insufficiency as the upfront layer of fluid particles approaches the removal threshold but this compensation does not seem promising. The result of this underestimation of pressure is the particle clustering at the outlet. Several ways have been examined to compensate for this insufficiency.

One of the practical and easily implementable trends to overcome this issue is to impose the pressure field to the last layers of the flow field. By doing so, there is no need to have the ghost layer in the outflow. However, this trend is not a physical one and does not vary during the simulation, and won't have a high accuracy in capturing the pressure field.

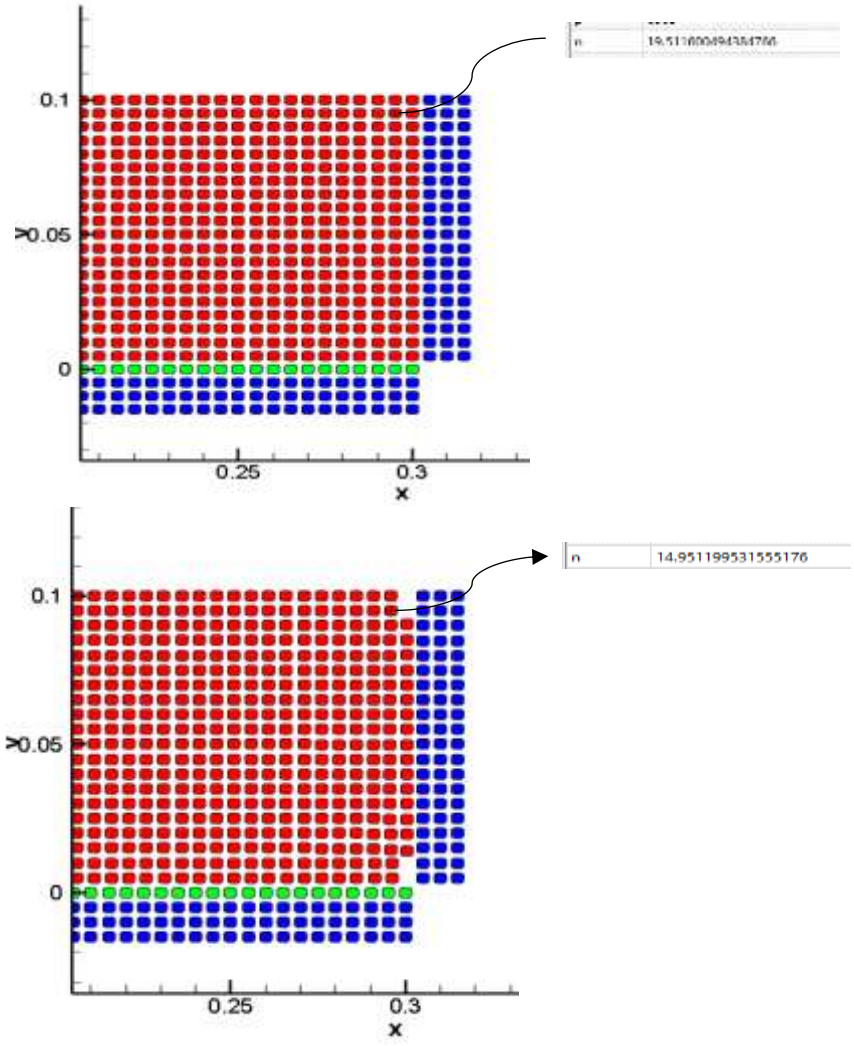

Figure 4.12 Frontier particles' particle number density drop after a particle elimination

The other way which is relatively hard to implement is to add an auxiliary amount to the particle number density of the frontier particles. Ideally, we would like to compensate for the sudden

removal of our frontier particle (particle B) with the ghost particle (Figure 4.13). The lack of particle number density that particle A senses due to particle B's disappearance is $w_1 = w(r_1, r_e)$.

We assume that the x-wise speed of all the particles in the support domain of our frontier particle is the same. In this case, if the particle A traverse x_l, then the amount of overestimation of particle number density due to the presence of motionless ghost particles will be as follows:

$$w_2 = \sum_{x=2}^{n} w(r_x, r_e) - \sum_{x=2}^{n} w(r'_x, r_e) \tag{4.1}$$

In which r'_x are the distances between the particle B with the ghost particles if they traverse x_l.

So we can compensate for this shortage by adding an auxiliary term w':

$$\begin{aligned} &w_1 = w_2 + w' \quad \rightarrow \quad w' = w_1 - w_2 \\ &w' = w(r_1, r_e) - \textstyle\sum_{x=2}^{n} w(r_x, r_e) + \sum_{x=2}^{n} w(r'_x, r_e) \end{aligned} \tag{4.2}$$

It should be noted that r_1 refers to the distance between particle B and particle A if it also traverses x_l.

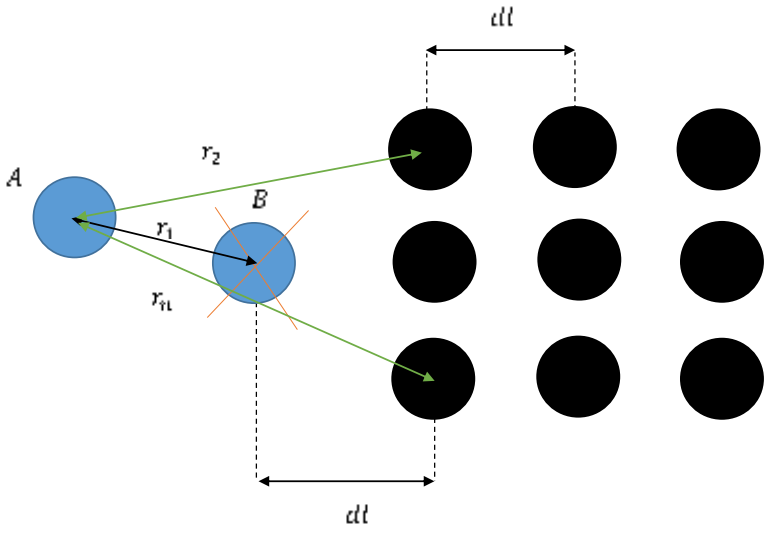

Figure 4.13 Particle elimination treatment

By adding an auxiliary amount to the particle number density of the frontier particles the shortage of particle number density caused by particle removals can be compensated.

Another trend to tackle this issue which is already implemented in this research is to use a weir at the end of the flume. The height of the weir should be enough to ensure the outflow does not face any altitude drop. This method is easily implementable by adding fixed wall particles at the end of the flume.

4.2.3 Results and analysis

Figure 4.14 shows the snapshots of the numerical simulations showing the evolution of ice mass. The first image shows the initial condition. It should be noted that the ice particles are distributed normally before the rigid floating ice sheet in order to save computational expenses. The increase in water level is noticeable. The discharge for the following snapshots was $48\ l/s$ and the SVP rheological model is implemented, however, there were no significant differences in the ice evolution by changing the rheological model.

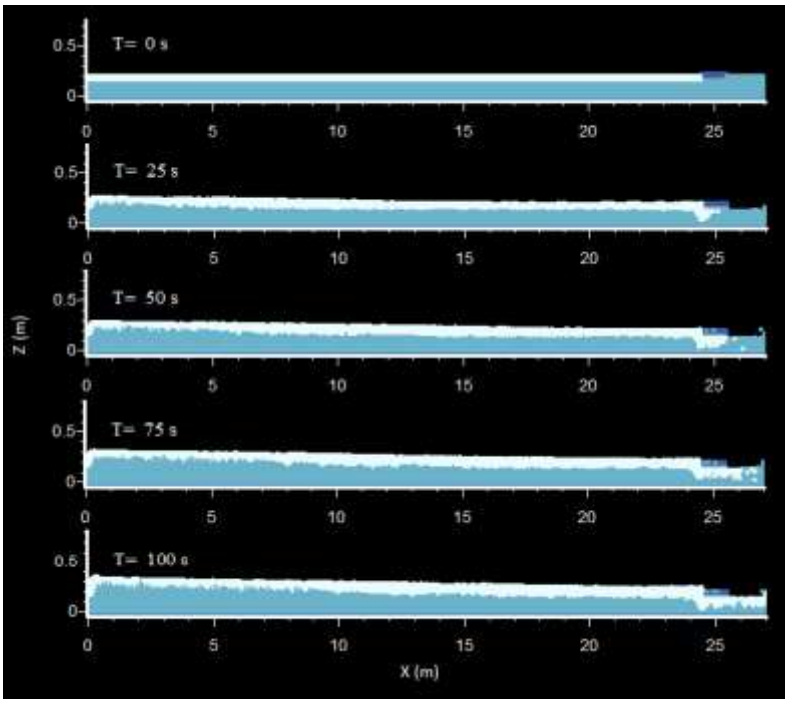

Figure 4.14 Experimental flume apparatus and the initial position of particles

By distributing the ice particles normally before the rigid floating ice sheet, the steady-state time turned out to be around 100 seconds which can be observed in Figure 4.15. This figure shows the non-dimensionalized ice thickness vs non-dimensionalized jam length for a discharge of $34\ l/s$. The non-dimensionalized position is the streamwise distance from the head of the flume divided by the length of the ice jam and the non-dimensionalized thickness of ice is the measured thickness at location x divided by the average jam thickness. As it can be inferred from Figure 4.15, The ice thickness and in general the simulation is steady at around 100s.

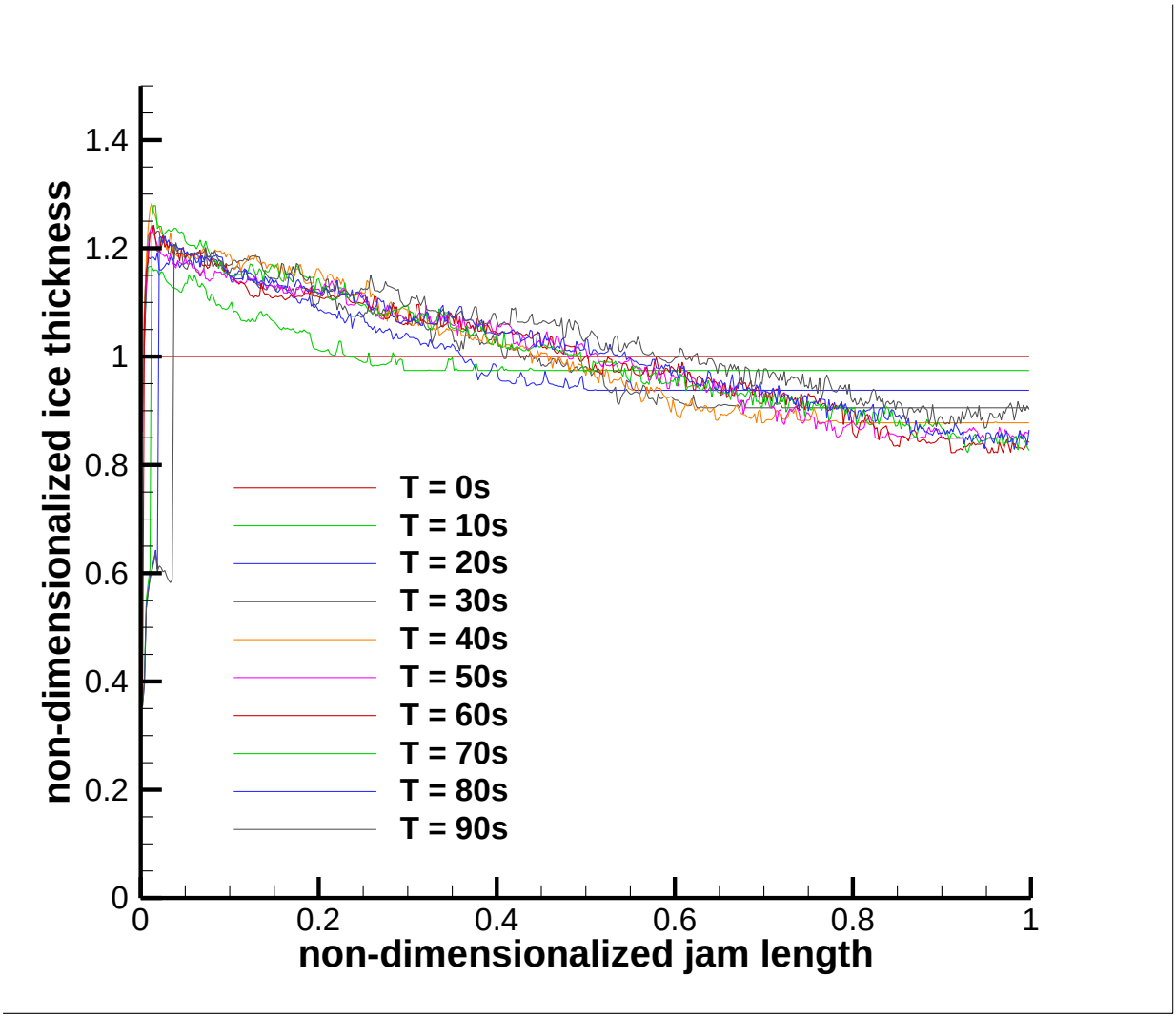

Figure 4.15 Non-dimensionalized thickness vs jam length evolution until steady state

To compare with the experimental results, the non-dimensional ice thickness versus the non-dimensional jam length in the steady-state condition with different discharges is validated in Figure 4.16. The results showed great agreement between the developed model and the experimental data for both rheological models proving the capability of the model.

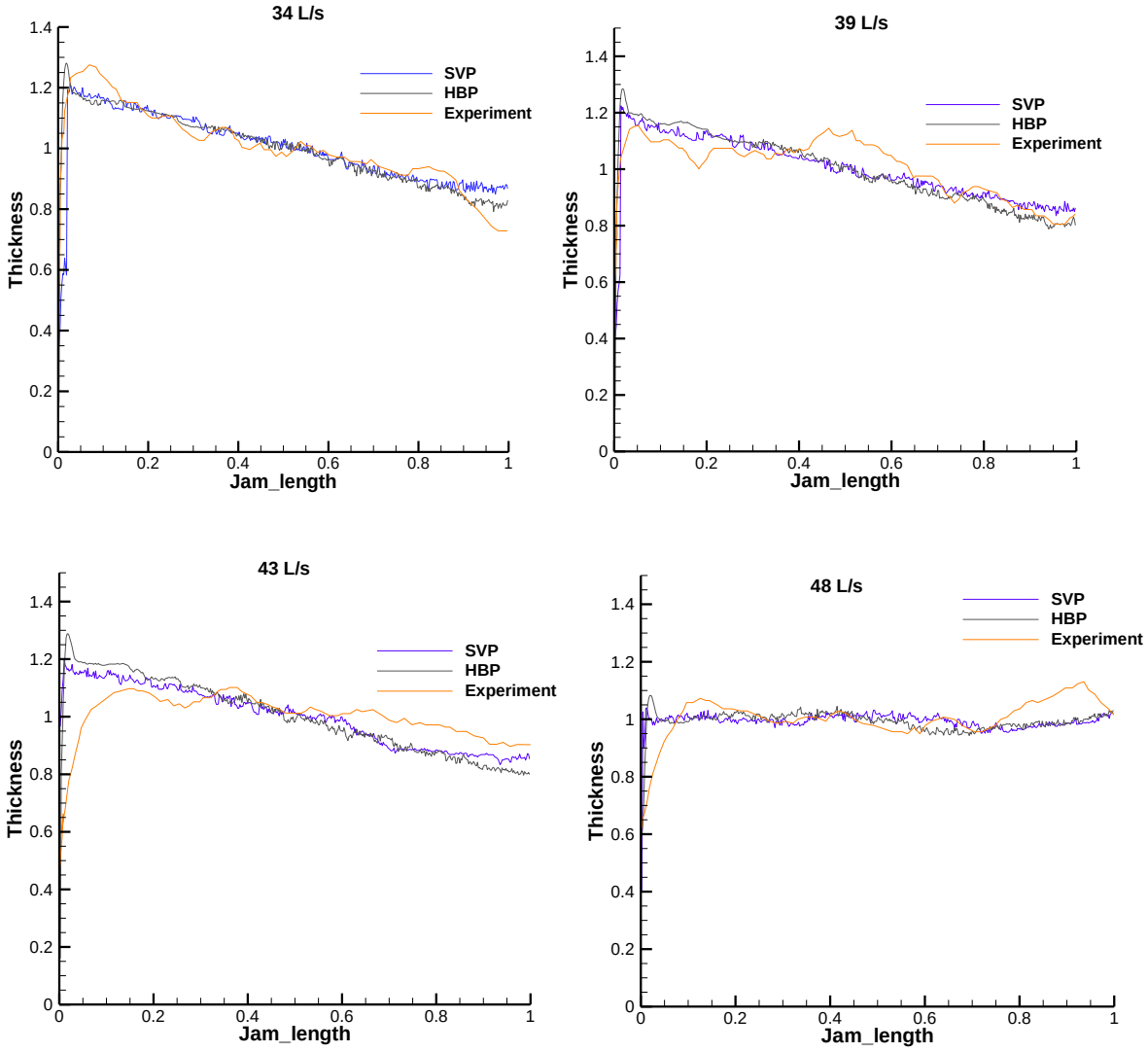

Figure 4.16 Comparison of the dimensionless plot of ice jam formation with different discharges

As indicated in Figure 4.16, the ice accumulation tended to be slightly thicker than the average near the head of the flume due to the entrainment and subsequent deposition of ice pieces and slightly thinner near the toe. In other words, we can see a more classical shape of ice jam in high discharges where the accumulation tends to be slightly thicker downstream. It is notable that the effect of turbulence is considerable in this simulation. Considering the average inlet speed of $0.25\frac{m}{s}$ and $0.3\,m$ as the diameter of the flume, the Reynolds number would be greater than the critical Reynolds number in the pipes which is around 2300. So involving turbulence models like the eddy viscosity models such as $k-\epsilon$ or $k-\omega$ or the LES-type sub-particle scale (SPS) turbulent model can augment the accuracy of the results. Like the other test case, there is a discrepancy between the simulation and the experiment. The actual experiment is in three dimensions whereas the simulation is in two dimensions in which the effect of the third dimension is neglected.

As a conclusion, both rheological models showed their capabilities in coupling with the Lagrangian particle-based method with the continuum assumption.

Chapter 5 CONCLUSION (AND RECOMMANDATIONS)

In order to simulate highly dynamic, large-scale cases like ice jams, the available models were investigated. Among them, a model which was known to be appropriate to handle large scales with a reasonable accuracy was designated. A continuum-based fully-Lagrangian model, based on the MPS numerical method, was developed for the simulation of ice-water dynamics. The non-Newtonian behavior of the ice continuum was described using two Visco-Plastic constitutive laws, i.e., the Standard Visco-Plastic (SVP) and the Herschel–Bulkley (HB). The developed model was validated and evaluated for the cases of punch-through test and ice jam formation, where the experimental and numerical results showed good compatibility. The results proved the capability of the developed model for the simulation of ice dynamic problems.

Regarding the accuracy of the rheological models, although the HB model was a bit more stable in small cases like punch through, both of them were reasonable enough to be coupled with the particle-based methods and I would say the SVP would be a great choice due to its simplicity in implementation. Of course, there are some discrepancies between the actual experiments and the developed model’s simulation of the evaluated test cases. One of these gaps was the dimension of the simulation. As the simulations done in this research were in two dimensions, the effects of the third dimension were neglected.

As a continuum-based model, the ice floes' size and their distribution are not explicitly used in the model, yet they are reflected in the rheological characteristics. However, one should note that the continuum assumption, requires the computational elements (here particles) to be larger than the physical discrete elements (here ice floes), which will negatively affect the numerical resolution (especially for the water phase).

A solution to this challenge, which can be considered for future research, is using a multi-resolution particle method, similar to the work of (Mojtaba Jandaghian & Shakibaeinia, 2022) on multiphase granular flows. Further investigation is recommended for more detailed parametrization of the rheological model and extending the application to three-dimensional cases. Also, since the developed code is based on CPU, it can be GPU accelerated which augments the run time. By doing so, more particles can be utilized and the effect of the resolution can also be investigated. Moreover, considering the effect of turbulence especially in the ice jamming test case can be done to augment the accuracy of the results.

In addition, to evaluate the continuum-based assumption and generally finding out the effectiveness of this assumption, the same test cases can be simulated by the DEM method and measure how much accuracy is being sacrificed to gain computational budget.

REFERENCES

Ahlkrona, J., & Shcherbakov, V. (2017). A meshfree approach to non-Newtonian free surface ice flow: Application to the Haut Glacier d'Arolla. *Journal of computational physics, 330*, 633-649.

Amaro, R. A., Cheng, L.-Y., & Buruchenko, S. K. (2021). A Comparison Between Weakly-Compressible Smoothed Particle Hydrodynamics (WCSPH) and Moving Particle Semi-Implicit (MPS) Methods for 3D Dam-Break Flows. *International Journal of Computational Methods, 18*(02), 2050036.

Atluri, S. N., & Zhu, T. (1998). A new meshless local Petrov-Galerkin (MLPG) approach in computational mechanics. *Computational mechanics, 22*(2), 117-127.

Bai, W., Zhang, T., & McGovern, D. J. (2017). Response of small sea ice floes in regular waves: A comparison of numerical and experimental results. *Ocean Engineering, 129*, 495-506.

Beltaos, S. (1995). *River ice jams*: Water Resources Publication.

Beltaos, S. (2010). *Assessing ice-jam flood risk: methodology and limitations.* Paper presented at the Proceedings of the 20th IAHR Inernational Symposium on Ice, Lathi, Finland.

Belytschko, T., & Black, T. (1999). Elastic crack growth in finite elements with minimal remeshing. *International journal for numerical methods in engineering, 45*(5), 601-620.

Belytschko, T., Krongauz, Y., Organ, D., Fleming, M., & Krysl, P. (1996). Meshless methods: an overview and recent developments. *Computer methods in Applied mechanics and Engineering, 139*(1-4), 3-47.

Benson, D. J. (1992). Computational methods in Lagrangian and Eulerian hydrocodes. *Computer methods in Applied mechanics and Engineering, 99*(2-3), 235-394.

Blockley, E., Vancoppenolle, M., Hunke, E., Bitz, C., Feltham, D., Lemieux, J.-F., . . . Rampal, P. (2020). The future of sea ice modeling: where do we go from here? *Bulletin of the American Meteorological Society, 101*(8), E1304-E1311.

Chiang, J. C., & Bitz, C. M. (2005). Influence of high latitude ice cover on the marine Intertropical Convergence Zone. *Climate Dynamics, 25*(5), 477-496.

Church, J. A., Clark, P. U., Cazenave, A., Gregory, J. M., Jevrejeva, S., Levermann, A., . . . Nunn, P. D. (2013). *Sea level change*. Retrieved from

Colony, R., Pritchard, R., & Pritchard, R. S. (1975). AIDJEX BULLETIN No. 30 November 1975.

Coon, M., Maykut, G., & Pritchard, R. (1974). Modeling the pack ice as an elastic-plastic material.

Crespo, A. J., Domínguez, J. M., Rogers, B. D., Gómez-Gesteira, M., Longshaw, S., Canelas, R., . . . García-Feal, O. (2015). DualSPHysics: Open-source parallel CFD solver based on Smoothed Particle Hydrodynamics (SPH). *Computer Physics Communications, 187*, 204-216.

Crespo, A. J. C. (2008). Application of the smoothed particle hydrodynamics model SPHysics to free-surface hydrodynamics. *Universidade de Vigo*.

Docquier, D., Massonnet, F., Barthélemy, A., Tandon, N. F., Lecomte, O., & Fichefet, T. (2017). Relationships between Arctic sea ice drift and strength modelled by NEMO-LIM3. 6. *The Cryosphere, 11*(6), 2829-2846.

Duan, G., Yamaji, A., & Koshizuka, S. (2019). A novel multiphase MPS algorithm for modeling crust formation by highly viscous fluid for simulating corium spreading. *Nuclear Engineering and Design, 343*, 218-231.

Dunne, T. (2006). An Eulerian approach to fluid–structure interaction and goal-oriented mesh adaptation. *International journal for numerical methods in fluids, 51*(9-10), 1017-1039.

Feltham, D. L. (2005). Granular flow in the marginal ice zone. *Philosophical Transactions of the Royal Society A: Mathematical, Physical and Engineering Sciences, 363*(1832), 1677-1700.

Feltham, D. L. (2008). Sea ice rheology. *Annu. Rev. Fluid Mech., 40*, 91-112.

Flato, G., & Gerard, R. (1986). Calculation of ice jam thickness profiles. *Journal of Hydraulic Research, 28*(6), 737-752.

Forsythe, G. E., & Wasow, W. R. (1960). Finite Difference Methods. *Partial Differential*.

Garg, S., & Pant, M. (2018). Meshfree methods: A comprehensive review of applications. *International Journal of Computational Methods, 15*(04), 1830001.

Gingold, R. A., & Monaghan, J. J. (1977). Smoothed particle hydrodynamics: theory and application to non-spherical stars. *Monthly notices of the royal astronomical society, 181*(3), 375-389.

Gotoh, H., & Khayyer, A. (2016). Current achievements and future perspectives for projection-based particle methods with applications in ocean engineering. *Journal of Ocean Engineering and Marine Energy, 2*(3), 251-278.

Gotoh, H., & Sakai, T. (2006). Key issues in the particle method for computation of wave breaking. *Coastal Engineering, 53*(2-3), 171-179.

Gutfraind, R., & Savage, S. B. (1998). Flow of fractured ice through wedge-shaped channels: smoothed particle hydrodynamics and discrete-element simulations. *Mechanics of materials, 29*(1), 1-17.

Healy, D., & Hicks, F. (2006). Experimental study of ice jam formation dynamics. *Journal of Cold Regions Engineering, 20*(4), 117-139.

Heimbach, P., Menemenlis, D., Losch, M., Campin, J.-M., & Hill, C. (2010). On the formulation of sea-ice models. Part 2: Lessons from multi-year adjoint sea-ice export sensitivities through the Canadian Arctic Archipelago. *Ocean Modelling, 33*(1-2), 145-158.

Hibler III, W. (1979). A dynamic thermodynamic sea ice model. *Journal of physical oceanography, 9*(4), 815-846.

Hopkins, M. A. (2002). Using DEM to model Arctic sea ice. In *Discrete Element Methods: Numerical Modeling of Discontinua* (pp. 374-379).

Hopkins, M. A., Frankenstein, S., & Thorndike, A. S. (2004). Formation of an aggregate scale in Arctic sea ice. *Journal of Geophysical Research: Oceans, 109*(C1).

Hopkins, M. A., & Thorndike, A. S. (2006). Floe formation in Arctic sea ice. *Journal of Geophysical Research: Oceans, 111*(C11).

Hopkins, M. A., & Tuthill, A. M. (2002). Ice boom simulations and experiments. *Journal of Cold Regions Engineering, 16*(3), 138-155.

Hu, X. Y., & Adams, N. A. (2006). A multi-phase SPH method for macroscopic and mesoscopic flows. *Journal of computational physics, 213*(2), 844-861.

Huang, X., & Garcia, M. H. (1998). A Herschel–Bulkley model for mud flow down a slope. *Journal of fluid mechanics, 374*, 305-333.

Hunke, E. C., & Dukowicz, J. K. J. J. o. P. O. (1997). An elastic–viscous–plastic model for sea ice dynamics. *27*(9), 1849-1867.

Hutter, N., & Losch, M. J. T. C. (2020). Feature-based comparison of sea ice deformation in lead-permitting sea ice simulations. *14*(1), 93-113.

Jandaghian, M., & Shakibaeinia, A. (2020). An enhanced weakly-compressible MPS method for free-surface flows. *Computer methods in Applied mechanics and Engineering, 360*, 112771.

Jandaghian, M., & Shakibaeinia, A. (2022). Fluid-driven granular dynamics through a consistent multi-resolution particle method. *arXiv preprint arXiv:2202.13950*.

Junior, R. A. A., Mellado-Cusicahua, A., Shakibaeinia, A., & Cheng, L.-Y. (2021). A fully Lagrangian DEM-MPS mesh-free model for ice-wave dynamics. *Cold Regions Science and Technology, 186*, 103266.

Khayyer, A., Gotoh, H., & Shimizu, Y. (2019). A projection-based particle method with optimized particle shifting for multiphase flows with large density ratios and discontinuous density fields. *Computers & Fluids, 179*, 356-371.

Khayyer, A., Tsuruta, N., Shimizu, Y., & Gotoh, H. (2019). Multi-resolution MPS for incompressible fluid-elastic structure interactions in ocean engineering. *Applied Ocean Research, 82*, 397-414.

Koshizuka, S., Nobe, A., & Oka, Y. (1998). Numerical analysis of breaking waves using the moving particle semi-implicit method. *International journal for numerical methods in fluids, 26*(7), 751-769.

Koshizuka, S., & Oka, Y. (1996). Moving-particle semi-implicit method for fragmentation of incompressible fluid. *Nuclear science and engineering, 123*(3), 421-434.

Kreyscher, M., Harder, M., Lemke, P., & Flato, G. M. (2000). Results of the Sea Ice Model Intercomparison Project: Evaluation of sea ice rheology schemes for use in climate simulations. *Journal of Geophysical Research: Oceans, 105*(C5), 11299-11320.

Lemieux, J.-F., Tremblay, B., Sedláček, J., Tupper, P., Thomas, S., Huard, D., & Auclair, J.-P. (2010). Improving the numerical convergence of viscous-plastic sea ice models with the Jacobian-free Newton–Krylov method. *Journal of computational physics, 229*(8), 2840-2852.

Lemieux, J. F., & Tremblay, B. (2009). Numerical convergence of viscous-plastic sea ice models. *Journal of Geophysical Research: Oceans, 114*(C5).

Leppäranta, M. (1993). A review of analytical models of sea-ice growth. *Atmosphere-Ocean, 31*(1), 123-138.

Lind, S. J., Rogers, B. D., & Stansby, P. K. (2020). Review of smoothed particle hydrodynamics: towards converged Lagrangian flow modelling. *Proceedings of the Royal Society A, 476*(2241), 20190801.

Lind, S. J., Xu, R., Stansby, P. K., & Rogers, B. D. (2012). Incompressible smoothed particle hydrodynamics for free-surface flows: A generalised diffusion-based algorithm for stability and validations for impulsive flows and propagating waves. *Journal of computational physics, 231*(4), 1499-1523.

Lindenschmidt, K.-E. (2017). RIVICE—a non-proprietary, open-source, one-dimensional river-ice model. *Water, 9*(5), 314.

Lindenschmidt, K.-E., Das, A., Rokaya, P., Chun, K., & Chu, T. (2015). *Ice jam flood hazard assessment and mapping of the Peace River at the Town of Peace River.* Paper presented at the 18th Workshop on the Hydraulics of Ice Covered Rivers.

Lindenschmidt, K.-E., Sydor, M., Carson, R., & Harrison, R. (2012). Ice jam modelling of the Lower Red River. *Journal of Water Resource and Protection, 4*(1), 1-11.

Lindsay, R., & Stern, H. (2004). A new Lagrangian model of Arctic sea ice. *Journal of physical oceanography, 34*(1), 272-283.

Liu, G.-R. (2009). *Meshfree methods: moving beyond the finite element method*: Taylor & Francis.

Liu, G.-R., & Liu, M. B. (2003). *Smoothed particle hydrodynamics: a meshfree particle method*: World scientific.

Liu, G. R., & Jerry, S. Q. (2003). A non-reflecting boundary for analyzing wave propagation using the finite element method. *Finite elements in analysis and design, 39*(5-6), 403-417.

Liu, R., Yan, J., & Li, S. (2020). Modeling and simulation of ice–water interactions by coupling peridynamics with updated Lagrangian particle hydrodynamics. *Computational Particle Mechanics, 7*(2), 241-255.

Liu, W. K., Jun, S., & Zhang, Y. F. (1995). Reproducing kernel particle methods. *International journal for numerical methods in fluids, 20*(8-9), 1081-1106.

Lucie, C., Nowroozpour, A., & Ettema, R. (2017). Ice jams in straight and sinuous channels: insights from small flumes. *Journal of Cold Regions Engineering, 31*(3), 04017006.

Lucy, L. B. (1977). A numerical approach to the testing of the fission hypothesis. *The astronomical journal, 82*, 1013-1024.

Mair, H. U. (1999). Hydrocodes for structural response to underwater explosions. *Shock and Vibration, 6*(2), 81-96.

Marrone, S., Colagrossi, A., Le Touzé, D., & Graziani, G. (2010). Fast free-surface detection and level-set function definition in SPH solvers. *Journal of computational physics, 229*(10), 3652-3663.

Massonnet, F., Fichefet, T., & Goosse, H. (2015). Prospects for improved seasonal Arctic sea ice predictions from multivariate data assimilation. *Ocean Modelling, 88*, 16-25.

Monaghan, J. (1989). On the problem of penetration in particle methods. *Journal of computational physics, 82*(1), 1-15.

Monaghan, J. J. (1994). Simulating free surface flows with SPH. *Journal of computational physics, 110*(2), 399-406.

Morse, B., Francoeur, J., Delcourt, H., & Leclerc, M. (2006). Ice control structures using piers, booms and nets. *Cold Regions Science and Technology, 45*(2), 59-75.

Nguyen, V. P., Anitescu, C., Bordas, S. P., & Rabczuk, T. (2015). Isogeometric analysis: an overview and computer implementation aspects. *Mathematics and computers in simulation, 117*, 89-116.

Nguyen, V. P., Rabczuk, T., Bordas, S., & Duflot, M. (2008). Meshless methods: a review and computer implementation aspects. *Mathematics and computers in simulation, 79*(3), 763-813.

Nodoushan, E. J., Shakibaeinia, A., & Hosseini, K. (2018). A multiphase meshfree particle method for continuum-based modeling of dry and submerged granular flows. *Powder Technology, 335*, 258-274.

Nolin, S., Roubtsova, V., Morse, B., & Quach, T. (2009). Smoothed particle hydrodynamics hybrid model of ice-jam formation and release. *Canadian Journal of Civil Engineering, 36*(7), 1133-1143.

Oveisy, A., Dibike, Y. B., Prowse, T. D., Beltaos, S., & de Goede, E. (2015). *2DH numerical simulation of ice dynamic during break up.* Paper presented at the CGU HS committee on river ice processes and the environment, 18th workshop on the hydraulics of ice covered rivers, Québec City, Canada, August.

Panteleev, G., Yaremchuk, M., Stroh, J. N., Francis, O. P., & Allard, R. (2020). Parameter optimization in sea ice models with elastic–viscoplastic rheology. *The Cryosphere, 14*(12), 4427-4451.

Papanastasiou, T. C. (1987). Flows of materials with yield. *Journal of rheology, 31*(5), 385-404.

Pathak, H., Burela, R. G., Singh, A., & VirSingh, I. (2015). *Thermo-elastic failure simulation of 3-D orthotropic composites by XFEM.* Paper presented at the AIP Conference Proceedings.

Polojärvi, A., Tuhkuri, J., & Korkalo, O. (2012). Comparison and analysis of experimental and virtual laboratory scale punch through tests. *Cold Regions Science and Technology, 81*, 11-25.

Pritchard, R. S. (1975). An elastic-plastic constitutive law for sea ice.

Rabczuk, T., & Belytschko, T. (2004). Cracking particles: a simplified meshfree method for arbitrary evolving cracks. *International journal for numerical methods in engineering, 61*(13), 2316-2343.

REED, R. J., & CAMPBELL, W. J. (1960). *Theory and observations of the drift of ice station Alpha*. Retrieved from

Ren, D., Sin, W.-J., Kim, D.-H., Park, J.-C., & Jeong, S.-Y. (2020). Particle-based Numerical Simulation of Continuous Ice Breaking Process around Wedge-type Model Ship. *Journal of the Society of Naval Architects of Korea, 57*(1), 23-34.

Rothrock, D. (1970). The kinematics and mechanical behavior of pack ice: The state of the subject. *AIDJEX Bull, 2*, 1-10.

Ruzin, M. (1959). The wind drift of ice in a heterogeneous pressure field. *Tr. Arkt. Antartkt. Inst, 226*, 123-135.

Rybak, O., & Huybrechts, P. (2003). A comparison of Eulerian and Lagrangian methods for dating in numerical ice-sheet models. *Annals of Glaciology, 37*, 150-158.

Sayeed, T., Colbourne, B., & Molyneux, D. (2018). Experimental and numerical investigation of wave induced forces and motions of partially submerged bodies near a fixed structure in irregular waves. *Ocean Engineering, 163*, 451-475.

Shakibaeinia, A., & Jin, Y.-C. (2011). MPS-based mesh-free particle method for modeling open-channel flows. *Journal of Hydraulic Engineering, 137*(11), 1375-1384.

Shakibaeinia, A., & Jin, Y.-C. (2012). MPS mesh-free particle method for multiphase flows. *Computer methods in Applied mechanics and Engineering, 229*, 13-26.

Shakibaeinia, A., & Jin, Y. C. (2010). A weakly compressible MPS method for modeling of open-boundary free-surface flow. *International journal for numerical methods in fluids, 63*(10), 1208-1232.

Shedbale, A., Singh, I., & Mishra, B. (2013). Nonlinear simulation of an embedded crack in the presence of holes and inclusions by XFEM. *Procedia Engineering, 64*, 642-651.

Shen, H. T., Su, J., & Liu, L. (2000). SPH simulation of river ice dynamics. *Journal of computational physics, 165*(2), 752-770.

Snelling, B. E., Collins, G. S., Piggott, M. D., & Neethling, S. J. (2020). Improvements to a smooth particle hydrodynamics simulator for investigating submarine landslide generated waves. *International journal for numerical methods in fluids, 92*(7), 744-764.

Spandan, V., Lohse, D., de Tullio, M. D., & Verzicco, R. (2018). A fast moving least squares approximation with adaptive Lagrangian mesh refinement for large scale immersed boundary simulations. *Journal of computational physics, 375*, 228-239.

Tandon, N. F., Kushner, P. J., Docquier, D., Wettstein, J. J., & Li, C. (2018). Reassessing sea ice drift and its relationship to long-term Arctic sea ice loss in coupled climate models. *Journal of Geophysical Research: Oceans, 123*(6), 4338-4359.

Tremblay, L.-B. (1999). A comparison study between two visco-plastic sea-ice models. In *Advances in Cold-Region Thermal Engineering and Sciences* (pp. 333-352): Springer.

Tsay, R.-J., Chiou, Y.-J., & Chuang, W.-L. (1999). Crack growth prediction by manifold method. *Journal of engineering mechanics, 125*(8), 884-890.

Tsuruta, N., Khayyer, A., & Gotoh, H. (2013). A short note on dynamic stabilization of moving particle semi-implicit method. *Computers & Fluids, 82*, 158-164.

Turcotte, B., & Morse, B. (2015). *Ice-induced flooding mitigation at St. Raymond, QC, Canada.* Paper presented at the 18th Workshop on the Hydraulics of Ice Covered Rivers, Quebec City, QC, Canada.

Vancoppenolle, M., Fichefet, T., Goosse, H., Bouillon, S., Madec, G., & Maqueda, M. A. M. (2009). Simulating the mass balance and salinity of Arctic and Antarctic sea ice. 1. Model description and validation. *Ocean Modelling, 27*(1-2), 33-53.

Violeau, D., & Leroy, A. (2014). On the maximum time step in weakly compressible SPH. *Journal of computational physics, 256*, 388-415.

Violeau, D., & Rogers, B. D. (2016). Smoothed particle hydrodynamics (SPH) for free-surface flows: past, present and future. *Journal of Hydraulic Research, 54*(1), 1-26.

Wang, J., Hua, J., Chen, P.-p., Sui, J., Wu, P., & Whitcombe, T. (2019). Initiation of ice jam in front of bridge piers—An experimental study. *Journal of Hydrodynamics, 31*(1), 117-123.

Wang, Z.-B., Chen, R., Wang, H., Liao, Q., Zhu, X., & Li, S.-Z. (2016). An overview of smoothed particle hydrodynamics for simulating multiphase flow. *Applied Mathematical Modelling, 40*(23-24), 9625-9655.

Xie, J., & Jin, Y.-C. (2016). Parameter determination for the Cross rheology equation and its application to modeling non-Newtonian flows using the WC-MPS method. *Engineering Applications of Computational Fluid Mechanics, 10*(1), 111-129.

Yan, X., Mohammadian, A., & Rennie, C. D. (2020). Numerical modeling of local scour due to submerged wall jets using a strict vertex-based, terrain conformal, moving-mesh technique in OpenFOAM. *International Journal of Sediment Research, 35*(3), 237-248.

Ye, T., Pan, D., Huang, C., & Liu, M. (2019). Smoothed particle hydrodynamics (SPH) for complex fluid flows: Recent developments in methodology and applications. *Physics of Fluids, 31*(1), 011301.

Zhang, C., Xiang, G., Wang, B., Hu, X., & Adams, N. A. (2019). A weakly compressible SPH method with WENO reconstruction. *Journal of computational physics, 392*, 1-18.

Zhang, Z., & Chen, Q. (2007). Comparison of the Eulerian and Lagrangian methods for predicting particle transport in enclosed spaces. *Atmospheric environment, 41*(25), 5236-5248.

Zienkiewicz, O. C., Taylor, R. L., & Zhu, J. Z. (2005). *The finite element method: its basis and fundamentals*: Elsevier.

APPENDIX A IAHR PAPER

26th IAHR International Symposium on Ice

Montréal, Canada – 19-23 June 2022

A continuum-based fully-Lagrangian model for ice-water dynamics

Mahyar Talebi, Mojtaba Jandaghian, Ahmad Shakibaeinia

Polytechnique Montreal University, Department of Civil Engineering

Montrèal, Canada

Mahyar.talebi@polymtl.ca, *Mojtaba.jandaghian@polymtl.ca* ,

Ahmad.shakibaeinia@polymtl.ca

Numerical methods for ice dynamics problems are either based on the discrete or continuum descriptions of the ice floes. While the discrete-based approaches, such as the Discrete Element Method (DEM), are very accurate, they are computationally expensive for large-scale problems, as they deal with individual ice floes. On the other hand, the continuum description offers scalability and computational affordability, by considering the assembly of ice parcels as a body of continuum and solving the conservation equations. In combination with the mesh-free Lagrangian (particle) numerical methods, such as Smoothed Particle Hydrodynamic (SPH) and Moving Particle Semi implicit (MPS), the continuum description can also offer accuracy and flexibility comparable to the discrete description. In this study, we propose an MPS Lagrangian numerical method for simulation of multiphase ice-water dynamics, based on continuum description of both ice and water, considered as non-Newtonian and Newtonian fluids, respectively. To predict the non-Newtonian behaviour of the ice continuum, we examine two Visco-Plastic constitutive laws, i.e., the Standard Visco-Plastic (SVP) and the Herschel–Bulkley (HB). The developed model is validated and evaluated for the cases of punch-through test, and ice jamming. Comparison with the experimental data shows the accuracy and reliability of the developed model.

River ice dynamics is the common problem of cold-regions rivers during the ice formation and breakup periods. The movement of ice floes, their interaction with river boundaries and hydraulic structures, and the possibility of jamming can impact many fluvial, environmental, and engineering processes. Particularly, the ice jamming can damage the fluvial infrastructures and block the natural flow causing significant water level rises and floods. Therefore, the prediction of river dynamics is an essential element of fluvial studies and flood risk assessment during ice periods. Recent efforts on numerical simulation of ice dynamics have focused on discrete description or continuum description of ice parcels. Discrete description (e.g., in Discrete Element Method, DEM) deals with individual ice parcels subject to macroscopic and microscopic force (Junior et al., 2021). Although the discrete methods are useful for the accurate analysis of ice dynamics, they are relatively computationally expensive and restricted to small-scale problems. In contrast, continuum description treats the ice material as a body of continuum and solves the conservation laws to predict the state of the system. The continuum approaches are computationally affordable for larger-scale problems.

While most of the past research on continuum-based modelling of ice dynamics has been using Eulerian mesh-based methods (Bai et al., 2017; Sayeed et al., 2018), Some recent efforts have been made toward the use of mesh-free Lagrangian (particle-based) methods. Mesh-free Lagrangian methods such as Smoothed Particle Hydrodynamics (SPH) and Moving particle-semi-implicit (MPS) are very flexible for simulating continuums with large interfacial deformations, therefore, are ideal for handling the complex dynamics of ice-water systems. (Gutfraind & Savage, 1998; Lindsay & Stern, 2004; Nolin et al., 2009; Oveisy, Dibike, Prowse, Beltaos, & de Goede, 2015; Shen et al., 2000) made the earliest efforts to use depth-averaged SPH (insemination with an Eulerian hydrodynamic model) for ice dynamic simulation. Similarly, (Oveisy et al., 2015) used a depth-averaged MPS technique that was in combination with a finite-volume technique. These hybrid models were based on the shallow flow assumption hence not appropriate for reproducing the dynamics of fast-flowing ice parcels. Continuum-based modelling also relies on appropriate rheological models to describe the internal stresses of the ice material. Past investigations on ice rheology have led to elastic-plastic and viscous-plastic models (Coon et al., 1974; Hibler III, 1979). Standard Visco-Plastic (SVP), and Granular material approach (GRAM) are two of the widely used visco-plastic models (Tremblay, 1999).

This paper aims at developing a fully-Lagrangian mesh-free model, based on the MPS method for continuum-based modelling of ice-water dynamics. MPS is used to solve the full dynamic Navier–Stokes equations for both water and ice phases. Various rheological models are used to predict the ice mechanical behavior. The developed model is validated for punch-through benchmark test, as well as ice jam formation in an experimental channel.

6.1 Methodology

6.1.1 Governing equations

Here we consider the ice-water computational domain as a multi-density multi-viscosity system and a single set of governing equations is solved for the entire flow field. The governing equation includes the conservation of mass and momentum (in a Lagrangian framework) and the equation of motion as:

$$\begin{cases} \frac{1}{\rho}\frac{\mathrm{D}\rho}{\mathrm{D}t} + \nabla.\mathbf{u} = 0 \\ \rho\frac{\mathrm{D}\mathbf{u}}{\mathrm{D}t} = \nabla.\boldsymbol{\sigma} + \mathbf{g} \\ \frac{\mathrm{D}\mathbf{r}}{\mathrm{D}t} = \mathbf{u} \end{cases} \tag{5.1}$$

where ρ, $\mathbf{u}$, $\boldsymbol{\sigma}$, $\mathbf{g}$, and $\mathbf{r}$ are density, velocity vector, total stress tensor, gravity acceleration, and position vector respectively. Using a mesh-free particle method, the solution domain is represented/discretized by the equal-size particles (i.e. computational nodes). The stress tensor is calculated using a rheological model.

The ambient fluid (water) is represented by the fluid-type particles, and the mixture of ice material and interstitial fluid is treated as a monophasic isotropic continuum and is represented by ice-type particles (**Figure 6.1**).

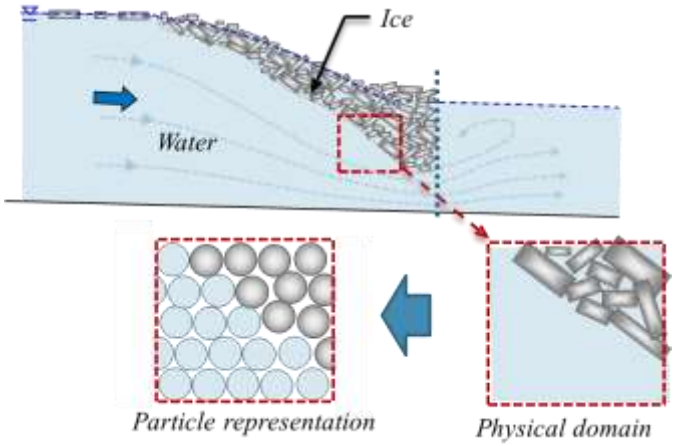

Figure 6.1 Particle-based representation of ice-water system

6.1.2 Rheological model

Here we examine two visco-plastic rheological models, the standard Visco-Plastic (SVP) (Hibler III, 1979) and Herschel-Bulkley (HB) generalized visco-plastic (Huang & Garcia, 1998) models. The SVP considers ice as a nonlinear viscous compressible fluid, for which the total stress tensor is calculated from:

$$\boldsymbol{\sigma} = 2\eta\mathbf{E}' - p\mathbf{I} + \left(\frac{p}{2} + \zeta E_I\right)\mathbf{I}$$

where (5.2)

$$\eta = \min\left(\frac{\zeta}{e^2}, \eta_{\max}\right), \quad \zeta = \min\left(\frac{p}{2\Delta}, \zeta_{\max}\right), \quad \Delta = \sqrt{E_I^2 + \left(E_{II}^2/e\right)^2}$$

in which $\boldsymbol{I}$ is the identity tensor, $\mathbf{E}'$ is the deviatoric strain rate tensor, p is a pressure term, ζ and η are nonlinear bulk and shear viscosities, and E_I and E_{II} are the first and second invariants of the strain rate tensor. The bulk and shear viscosity define the rheology term which depends on the yield curve and the flow rule. As suggested by Hibler (1979), the elliptical yield curve (where e is the ellipse aspect ratio) is used in SVP model. The stress tensor in the Herschel-Bulkley (HB) model is defined as:

$$\boldsymbol{\sigma} = 2\eta\mathbf{E}' - p\mathbf{I}$$
$$\textit{where}$$
$$\eta = \min\left(\frac{\tau_y}{2\sqrt{E_{II}}} + \mu_0\left(2\sqrt{E_{II}}\right)^{\beta-1}, \eta_{\max}\right) \tag{5.3}$$

where τ_y is the yield stress given by Mohr-Coulomb, and μ_0 and β are consistency and behaviour indexes. One can consider GRAM model an especial case of HB model with μ_0=0.

6.1.3 MPS discretization

Here a weakly-compressible MPS (WC-MPS) method (Shakibaeinia & Jin, 2010) is employed. In MPS, the continuum is represented by a set of mobile particles. The technique is based on weighted averaging of quantities, vectors and derivatives. Each particle i with position vector $\mathbf{r}_i$, interacts with its neighboring particle j in using a weight function, $W(r_{ij}, r_e)$, where $r_{ij}=|\mathbf{r}_j-\mathbf{r}_i|$ and r_e are distance between particles and effective radius, respectively. The pressure gradient term and the divergence-free viscous term are given by (Shakibaeinia & Jin, 2012).

$$\langle\nabla p\rangle_i = \frac{d}{n_0}\sum_{j\neq i}\left(\frac{p_j - \hat{p}_i}{r_{ij}^2}\mathbf{r}_{ij}W\left(x_{ij}, r_e\right)\right);\quad \hat{p}_i = \min_{j\in J}(p_i, p_j);\ J = \left\{j : W\left(r_{ij}, r_e\right) > 0\right\}$$
$$\left\langle\nabla\left(\mu\nabla\cdot\mathbf{u}\right)\right\rangle_i = \frac{4d}{\lambda n_0}\sum_{j\neq i}\left(\frac{\mu_i\mu_j}{\mu_i+\mu_j}\left(\mathbf{u}_j - \mathbf{u}_i\right)W\left(r_{ij}, r_e\right)\right) \tag{6.4}$$

where n_0 is particle number density, and d, number of space dimensions, The MPS approximation of the strain rate tensor, $\mathbf{E}$, can be written as:

$$\mathbf{E}_i = \begin{bmatrix} \dot{e}_{xx} & \dot{e}_{xy} \\ \dot{e}_{yx} & \dot{e}_{yy} \end{bmatrix}_i = \frac{1}{n_0} \begin{bmatrix} 2\sum_{j^i i}\left(\frac{u_{ij}x_{ij}}{r_{ij}^2}W_{ij}\right) & \sum_{j^i i}\left(\frac{u_{ij}y_{ij}+v_{ij}x_{ij}}{r_{ij}^2}W_{ij}\right) \\ \sum_{j^i i}\left(\frac{u_{ij}y_{ij}+v_{ij}x_{ij}}{r_{ij}^2}W_{ij}\right) & 2\sum_{j^i i}\left(\frac{v_{ij}y_{ij}}{r_{ij}^2}W_{ij}\right) \end{bmatrix} \quad (5.5)$$

A fractional-step time integration methods is employed to solve the equations. As in the WC-MPS (Shakibaeinia & Jin, 2010) the fluids are assumed to be weakly compressible, and the Tait's equation of state is used for prediction of the pressure.

6.1.4 Punch through simulation

The developed model is applied and validated with an experimental punch through test case (Polojärvi et al., 2012). A water tank is filled with water and artificial ice rubbles and a flat indenter platen moves downward through the rubble mass (**Figure 6.2**). The W_b is the instrumented wall width, which is movable in the experiment but here we have fixed walls with $2.5\,m$ width. The initial particle representation of the domain is shown in **Figure 6.2**. To simulate this test case in two dimensions, total number of 20,000 particles are implemented. The indenter moves at the speed of $10\,mm/s$. **Figure 6.3** shows the snapshot of the simulated particle configuration for $y_i = 80\,mm$ and $y_i = 240\,mm$ (y_i being the indenter's displacement from the origin). The ratio of ice particles displacement to the indenter's displacement (as an indication of rubble mass deformation) is compared with the experimental data in **Figure 5.4**, showing a good compatibility. Also, the volume of displaced ice particles simulated using SVP and HB rheological models are compared with the experimental values in **Figure 6.5**. Here the HB model shows a trend closer to that of experiment than the SVP model.

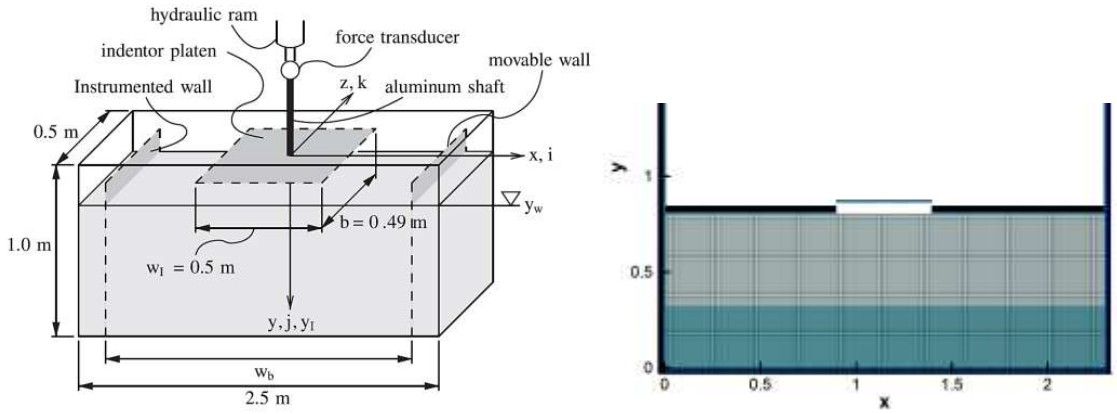

Figure 6.2 Experimental set up (Polojärvi et al., 2012) and initial position of particles in the numerical model

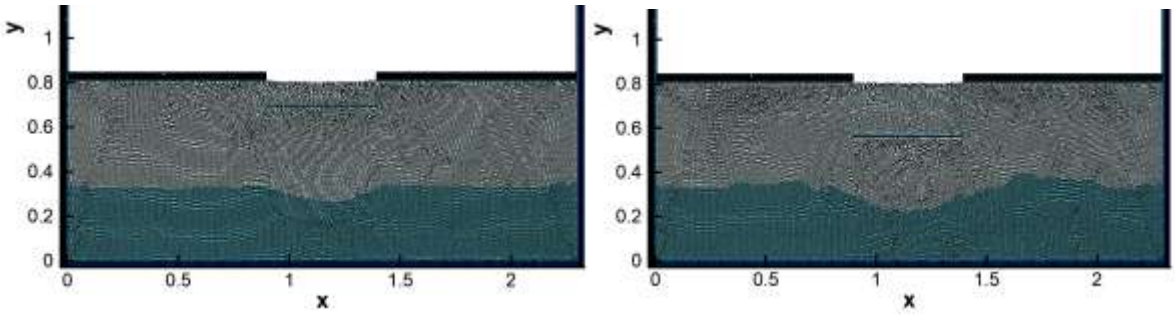

Figure 6.3 Position of ice and water particles in $y_i = 80\ mm$ and $y_i = 240\ mm$

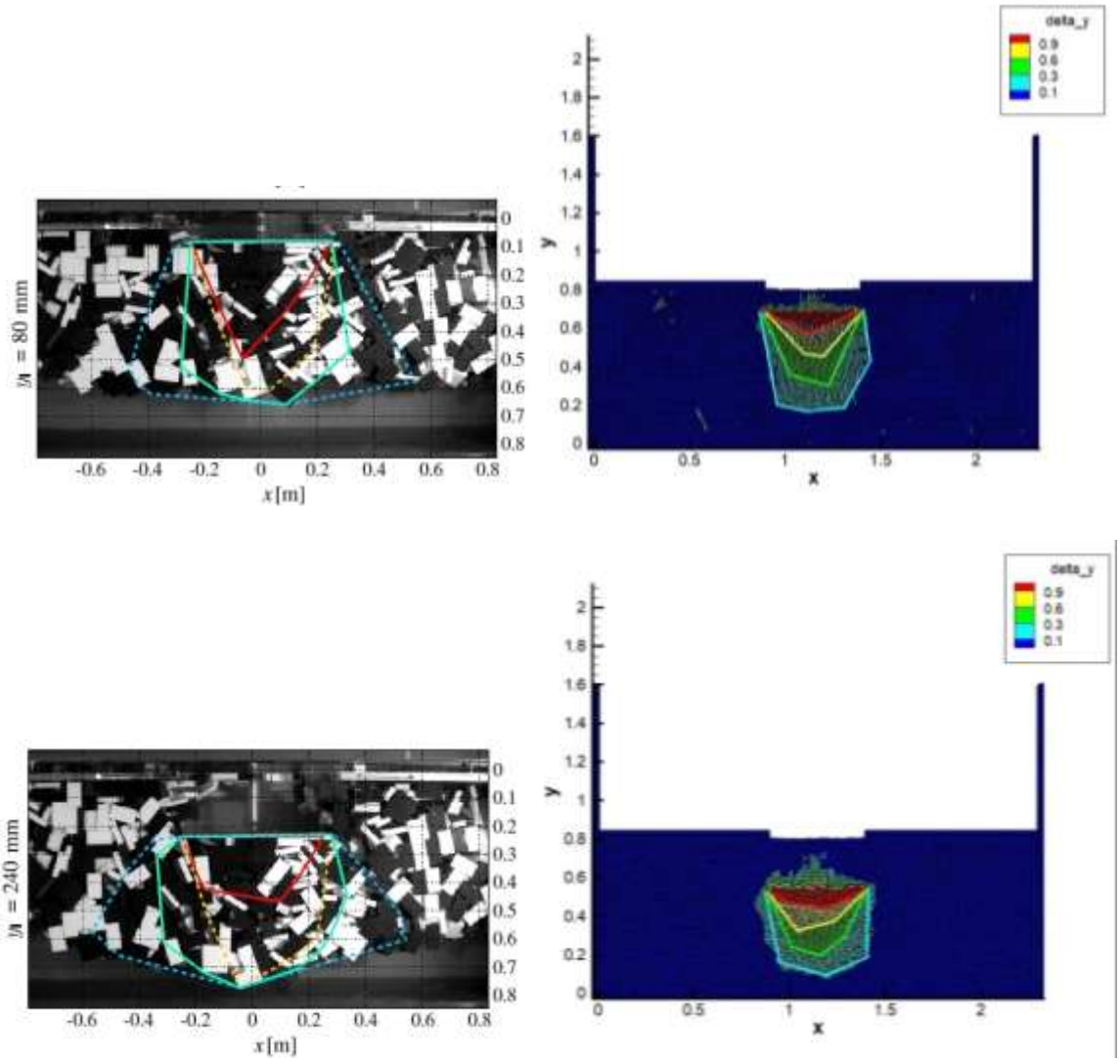

Figure 5.4 Deformation of particles based on the ratio to the indenter's displacement. Left: experimental results, Right: numerical results.

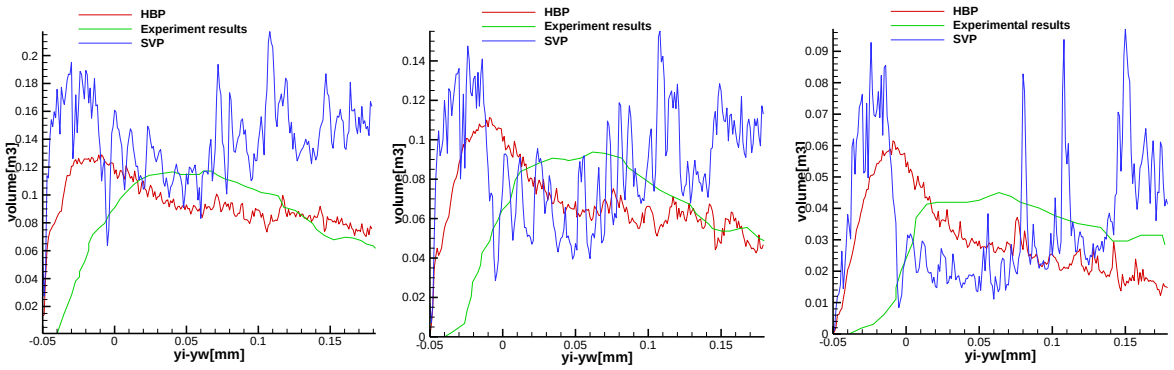

Figure 6.5 Volume of displaced ice particles with three vertical velocities v_y=2, 5 *and* 9 mm/s

6.1.5 Ice jam simulation

Next we apply and evaluate the developed model for a case of ice jam formation based on the experiments of (Healy & Hicks, 2006). The experiments were carried out in $32m$ long, $0.91m$ high sidewalls and $1.22m$ width recirculating flume. A sheet of plywood is positioned at $24m$ downstream of the flow to simulate an intact ice cover and initiate the ice jamming. For this test, discharges of $35-65\ L/s$ are supplied to the head tank (**Figure 5.6**). The experiments are done with and without a wire mesh to block the ice parcels, however, here we only simulate the case without the wire mesh. **Figure 5.7** shows the snapshots of the numerical simulations showing the evolution of ice mass. To compare with the experimental results, the non-dimensional ice thickness versus the non-dimensional jam length in steady-state condition is validated in **Figure 5.8**. The results showed great agreement between the developed model and the experimental data for both rheological models proving the capability of the model.

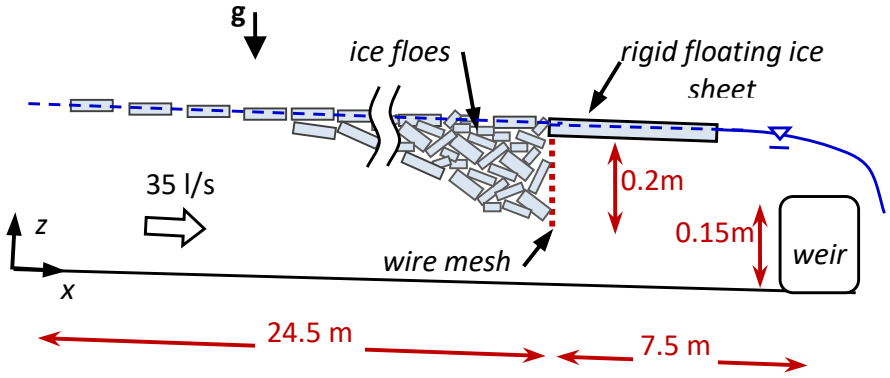

Figure 5.6 Experimental configuration of the ice jam formation case

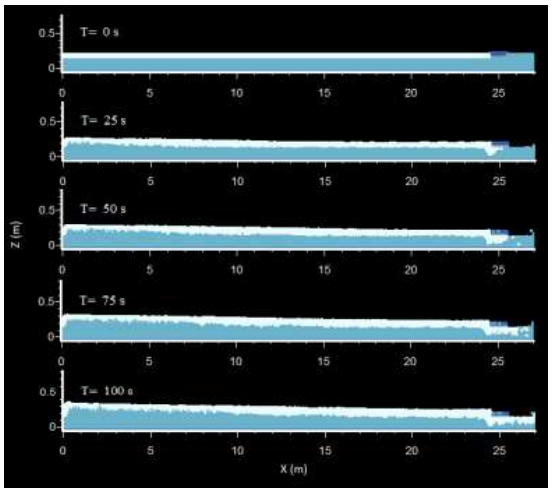

Figure 5.7 Experimental flume apparatus and the initial position of particles

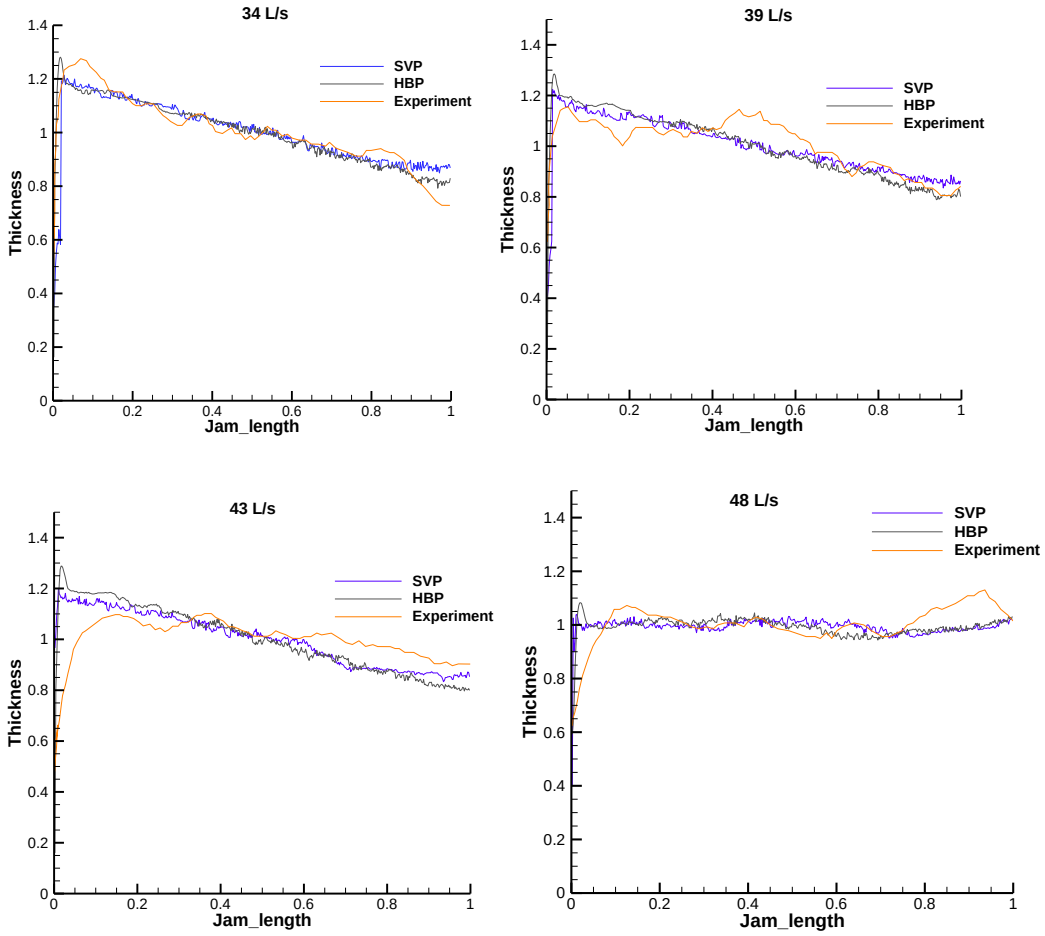

Figure 5.8 Comparison of dimensionless plot of ice jam formation with different discharges

6.2 Conclusion

A continuum-based fully-Lagrangian model, based on the MPS numerical method, was developed for the simulation of ice-water dynamics. The non-Newtonian behaviour of the ice continuum were described using two Visco-Plastic constitutive laws, i.e., the Standard Visco-Plastic (SVP) and the Herschel–Bulkley (HB). The developed model is validated and evaluated for the cases of punch-through test and ice jam formation, where the experimental and numerical results showed a good compatibility. The results proved the capability of the developed model for simulation of ice dynamic problems. As a continuum-based model, the ice floes size and its distribution are not explicitly used in the model, yet they are reflected in the rheological characteristics. However, one should note that the continuum assumption, requires the computational elements (here particles) to be larger than the physical discrete elements (here ice floes), which will negatively affect the numerical resolution (especially for the water phase). A solution to this challenge, which can be considered for the future research, is using a multi-resolution particle method, similar to the work of (Mojtaba Jandaghian & Shakibaeinia, 2022) on multiphase granular flows. Further investigation is recommended for more detailed parametrization of the rheological model and extending the application to three-dimensional cases.